2011

Transfer Length Measurements For Different Metallization Options And Processing Of Gallium Tin Zinc Oxide (Gszo) Tfts

Shereen. Farhana
North Carolina Agricultural and Technical State University

TRANSFER LENGTH MEASUREMENTS FOR DIFFERENT METALLIZATION OPTIONS AND PROCESSING OF GALLIUM TIN ZINC OXIDE (GSZO) TFTS

by

Shereen Farhana

A thesis submitted to the graduate faculty
in partial fulfillment of the requirements of the degree of
MASTER OF SCIENCE

Department: Electrical and Computer Engineering
Major: Electrical Engineering
Major Professor: Professor Shanthi Iyer

North Carolina A & T State University
Greensboro, North Carolina
2011

School of Graduate Studies
North Carolina Agricultural and Technical State University

This is to certify that the Master's thesis of

Shereen Farhana

has met the thesis requirements of
North Carolina Agricultural and Technical State University

Greensboro, North Carolina
2011

Approved by:

_____	_____
Dr. Shanthi Iyer Major professor	Dr. Ward J. Collis Committee member
_____	_____
Dr. Clinton B. Lee Committee member	Dr. John C. Kelly Department chairperson

_____
Dr. Sanjiv Sarin
Dean of Graduate Studies

DEDICATION

I would like to dedicate this thesis to my grandmother and parents as this journey of my entire academic career would not have been possible without their constant support and inspiration.

BIOGRAPHICAL SKETCH

Shereen Farhana was born on February 1st, 1985 in Dohar, Dhaka, Bangladesh. She was raised in the city of Dhaka. She received her Bachelor of Science degree in Computer Science and Engineering from Jahangir University in Bangladesh. She is currently a candidate for the Master of Science degree in Electrical and Computer Engineering.

ACKNOWLEDGEMENTS

I would like to express my gratitude to my advisor, Prof. Shanthi Iyer for her guidance and encouragement throughout this work. Special thanks to Dr. Ward J. Collis and Dr. J. Lewis from RTI, International for their critical input that allowed me to solve the technical problems at different stages of the research. I appreciate Dr. Clinton Lee for being the committee member of the thesis. I am also thankful to Dr. Jia Li, Tanina Bradley, Robert Alston, Adam Bowen and Sai Krishna Ojha for their prompt support in the laboratory. ARO funding (Grant No. W911NF-04-2-0051 and W911NF-10-1-0316), with Dr. Michael Gerhold being its technical monitor, is greatfully acknowledged.

TABLE OF CONTENTS

LIST OF FIGURES

FIGURES **PAGE**

LIST OF TABLES

TABLES **PAGE**

KEYS TO SYMBOLS

Si	Silicon
TFT	Thin film transistor
AOS	Amorphous oxide semiconductor
IGZO	Indium gallium zinc oxide
Ar	Argon
SiO_2	Silicon di-oxide
V_T	Threshold voltage
GSZO	Gallium tin zinc oxide
ZnO	Zinc oxide
PAC	Photoactive compound
HDMS	Hexamethyldisilxane
PEB	Post exposure baking
DI water	Deionized water
N_2	Nitrogen
A^o	Angstrom
TLM	Transfer length method
R_c	Contact resistance
ρ_c	Specific contact resistance
R_s	Sheet resistance
I	Current

V	Voltage
R_T	Total resistance
A_c	Contact area
P	Resistivity
T	Thickness
Z	Width of the contact pad
L_T	Transfer length
d	Spacing between the contact pads
Al	Aluminium
Au	Gold
Ti	Titanium
Pt	Platinum
nm	Nanometer
μm	Micrometer
r.p.m	Rotation per minute

ABSTRACT

Farhana, Shereen. TRANSFER LENGTH MEASUREMENTS FOR DIFFERENT METALLIZATION OPTIONS AND PROCESSING OF GALLIUM TIN ZINC OXIDE (GSZO) TFTS. (**Major Advisor: Professor Shanthi Iyer**). North Carolina Agricultural and Technical State University).

Transfer length measurements for various metal contacts on gallium tin zinc oxide film have been performed in this work to determine the specific contact resistivity. The investigated contacts are Al (100nm), Ti (20nm)/Al (30 nm)/Au (100nm) and Al (30nm)/ Au (50nm) and Al (30nm)/ Pt (50nm). The contacts were annealed after metal deposition at 250^{o}C in nitrogen ambient for different durations. The effect of intervals of post deposition annealing on the electrical property of the contacts have also been studied. The processing of thin film transistor (TFT) on gallium tin zinc oxide film has also been studied. The parameters attempted at stages of the processing and the comparisons between the corresponding outcomes have been shown. Finally, improved TFT patterns have been demonstrated for the processing conditions thus optimized.

CHAPTER 1

INTRODUCTION

The metal semiconductor contacts are important considerations in the fabrication of semiconductor devices. The contact quality has significant impact on the electrical characteristics of the device. Hence, the determination of the contact characteristics is very imperative to improve the quality of the contacts. Contact resistivity calculations of different metal on gallium tin zinc oxide (GSZO) film are carried out in this work. The resistance measurement technique used for this purpose is transfer length method. The metals used for developing contacts on film are Al(100nm), Ti(20nm)/Al(30nm)/Au(100nm), Al(30nm)/Au(50nm) and Al (30nm)/Pt(50nm) [1-4] . The best contact thus identified has been shown to improve the performance of the semiconductor device namely, thin film transistor (TFT).

A thin-film transistor is a field effect transistor produced by depositing a thin layer of film on a dielectric layer. The metal contacts are made on the active layers that act as source and drain. The film provides the active layer to form channel between the electrodes (source and drain). An extensive research on thin film transistors fabrication has been carried out as these are the elemental components for microelectronics [5] . Thin film transistors have aided in the evolution of flat- panel displays (FPDs) production [6]. The improved fast image quality and lower requirements of amount of charge have been possible by TFTs. Various materials have been investigated to enhance

electrical characteristics to make devices more effective to meet the emerging technological demand.

Silicon (Si) is commonly used as semiconductor material for producing TFT. Si has different crystalline states of semiconductors such as amorphous silicon [7], microcrystalline silicon and polycrystalline silicon [6]. These various states have also been used to control the characteristics of the TFTs. Apart from Si, some other compound semiconductor materials such as Cadmium Selenide [8] have been used to fabricate the TFTs. Metal oxides, for example, Zinc Oxides [9] are used to develop transparent active layers in TFTs. Fully transparent TFTs can be produced by using transparent electrodes like Indium Tin oxide (ITO) [10]. The various amorphous oxide semiconductors (AOSs) are widely examined candidates of TFT fabrication due to their favorable electrical performance. Amorphous indium gallium zinc oxide (a-IGZO) gives better mobility(10 cm^2/ Vs) than the hydrogenated amorphous silicon [7] . Amorphous indium zinc oxide (a-IZO) is a comparatively low cost and exhibits better electrical properties. The electron mobility (22.7 cm^2/ Vs) and threshold voltage are found to be higher than the a-IGZO [11]. Currently, indium has been replaced by tin which is abundant in quantity and less expensive [12] . Amorphous gallium tin zinc oxide (a-GSZO) yields TFTs of greater electron mobility (24.6 cm^2/ Vs) [12] than all the previously mentioned systems. This thesis reports a standard fabrication process of a-GSZO TFTs that yield desirable characteristics. A literature review on various resistance measurement methods and the TFT fabrication process have been discussed in chapter 2.

Experimental details for four probe method are presented in chapter 3. The instrumentation and steps of fabrication process for TFT production have been stated briefly.

Chapter 4 consists of data acquired using the transfer length measurements on different contacts. This section also shows of the fabrication process steps attempted with different parameter set up followed by the complete analysis of the results.

Chapter 5 presents the conclusion and also areas for the work to be expanded upon.

CHAPTER 2

LITERATURE REVIEW

Semiconductor devices like thin film transistors consist of numerous contacts. Different types of contacts such as metal-semiconductor and semiconductor-semiconductor are used in the devices. Between the two types, metal-semiconductor is the commonly used one. Braun in 1974 first discovered the metal-semiconductor contact resistance which led to more precise understanding of semiconductor device characteristics [13]. Contact resistance has played very important role to control the characteristics of the devices like avoiding the deterioration of the device performance as well as alternating the electrical properties [14] such as, current-voltage characteristics. Total resistance of the contact is a sum of several resistance components, such as, the contact resistance (R_c), the specific contact resistivity (ρ_c) and the sheet resistance (R_s). In this chapter, various contact resistance measurement techniques and the reason for choosing transfer length method over others have been explained. The literature survey on fabrication of thin film transistors has also been reported.

2.1 Contact Resistance Measurement by Transfer Length Method (TLM)

Various contact resistance measurement test structures have been examined [15-19]. Two terminal [20] , three terminal [21], four terminal [22-23] and six terminal [24] are considered to be the basic methods of the contact resistance measurements. Most of the test structures are able to extract the specific contact resistance [16] that can explain

the metal semiconductor interface resistance to some extent. Among all the contact resistance methods, the most complete resistance profile of the contacts is given by the transfer length method (TLM). Hence, the transfer length method is used to measure the various resistance parameters in this thesis work. Four probe method has been used to measure the total resistance between the contacts. The four probe measurement system is more reliable than other method (two-probe method) due to its elimination of parasitic capacitance [25]. Different test structures and a literature survey on contact resistance measurements of metal and GSZO film using the Transfer Length Method [15] are the subjects of this section.

2.1.1. Two-terminal method

Two terminal method was used to measure the contact resistances of large contact areas. This method is considered to be the oldest one and less complicated one to measure contact resistance of large area of ~ 1 cm^2 [26]. Two contacts of similar area, A_c were used and a current of I was passed vertically through the sample. The current could be passed laterally [27] but the structure became complex [28]which made measurements difficult .The voltage V was measured across the two contacts. The total resistance, R_T was thus measured from the Ohm's law, R_T= V/I. The semiconductor had a resistivity of ρ. The pictorial description of the test structure is presented in the Figure 2.1.

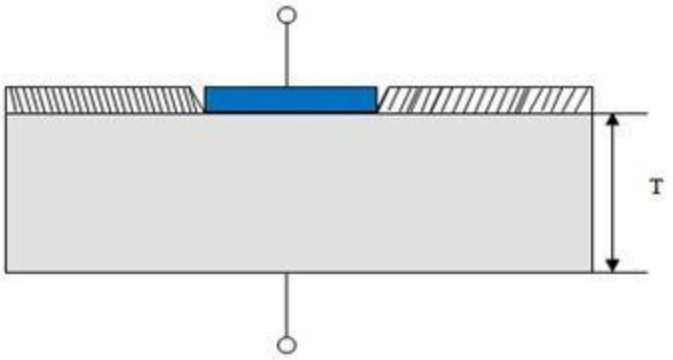

Figure 2.1. Test structure for two terminal method

The total resistance measured from the test structure was,

$$R_T = 2\,R_c + (\rho T / A_c) \tag{2.1}$$

The contact resistance R_c was obtained from the above equation and it was

$$R_c = (R_T - \rho T / A_c) / 2 \tag{2.2}$$

The specific contact resistivity ρ_c was calculated for the uniform current flow from the following expression,

$$\rho_c = R_c * A_c \tag{2.3}$$

Cox and Stack [20] extended the two terminal method by adding a small top contact and a large bottom contact. Two parameters, spreading resistance under the top contact (R_{sp}) and the bottom contact (R_o) resistance were included in the new two terminal method that contributed to the total resistance which is expressed in the following expression.

$$R_T = R_{sp} + R_c + Ro \tag{2.4}$$

The spreading resistance is dependent on the radius (r) of the circular top contact and the sample thickness (T) [20].

$$R_{sp} = [\rho / (2 * \pi * r)] \arctan [(2*T) / r] \quad (2.5)$$

The expression of the resistance of top contact with respect to the specific contact resistivity was written as

$$R_c = \rho_c / A_c = \rho_c / \pi * r^2 \quad (2.6)$$

The contact resistance is dependent on the difference of the total resistance and the spreading resistance, as the resistance of the bottom contact is very low. The bottom contact has comparatively large area than the top contact that makes the bottom contact resistance negligible. The two terminal methods works good for small contact area.

The diameter of the top contact can be varied in another approach of the two terminal method [29]. The contact resistance R_c is calculated from the expression 2.4. The total resistance R_T can be obtained from the experimental data. Then R_T is plotted as a function $1/R_c$. The specific contact resistance ρ_c is calculated from the slope of the plot.

The inadequacy of two terminal method is the inability to deal with sheet resistance efficiently and the specific contact resistance cannot be determined accurately [30] .

2.1.2 Three terminal contact resistance method

The three terminal contact resistance measurements utilize three contact pads of the same dimensions on a substrate with different spacing between the contacts shown in Figure 2.2. The total resistance can be measured from the following expression given as

$$R_{Ti} = R_s * d_i / Z + 2*R_c \quad (2.7)$$

where i is for 1 or 2. R_{T1} is measured across the first two contact pads and R_{T2} is between the second and third contacts. R_c can be extracted from the above two expressions which leads the equation 2.8.

$$R_c = (R_{T2}*d_1 - R_{T1}*d_2) / 2 * (d_1 - d_2) \quad (2.8)$$

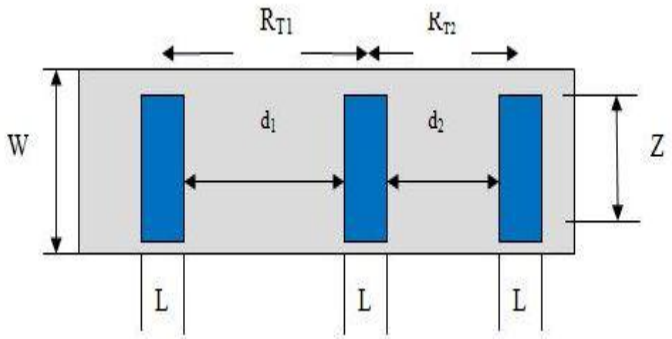

Figure 2.2. Test structure for three terminal contact resistances

The contact resistance is not dependent on the sheet resistance of the substrate which is considered to be the main advantage of this method. But reliable results are not provided by this method when the contact resistance is very low. The contact resistance result is dependent on the difference of the two spacing; a negative contact resistance value can be given by this measurement technique if the spacing between the first two contact pads is greater than the following two contact pads. Also, specific contact resistivity cannot be extracted from this method.

Current crowding was observed in the contacts proposed by Kennedy and Murley [31]. Current crowding happens due to comparatively more electron density near the edge of the emitter compared to the other region. The lateral voltage drop between the edge of

the emitter and the base causes high electron density near the edge of the emitter and the current also gets crowded near the edge. This leads to the non-uniform emitter current as well as non-uniform base current [32]. Zero contact resistance was assumed for their contacts and the actual contact length where the current was flowing to metal to semiconductor and semiconductor to metal was taken from the thickness of the semiconductor sheet. Considering the current crowding and specific contact resistivity transmission line model (TLM) was developed [18].

2.1.3. Transmission line model

Transmission Line Model was first used by Murrmann and Widmann to determine the contact and sheet resistance [21]. Both linear and concentric test structures could be used for the transmission line model [33].Extension of transmission line model was developed by Berger considering the contact resistance and layer sheet resistance to be nonzero and semiconductor sheet thickness to be zero [18, 34-35] . According to the transmission line model, the contact resistance can be calculated from the following expression [18]

$$R_c = (R_s * \rho_c)^{1/2} \coth (L/L_T) \tag{2.9}$$

where length of the contact and the transfer length are indicated by L and L_T respectively.

$$L_T = (\rho_c / R_s)^{1/2} \tag{2.10}$$

For $L \leq 0.5\ L_T$, equation 2.9 can be solved as

$$R_c = \rho_c / (L*Z) \tag{2.11}$$

For $L \geq 1.5\ L_T$, R_c can be written as

$$R_c \approx \rho_c / (L_T*Z) \tag{2.12}$$

Contact end resistance can be achieved (Figure 2.3) by applying current in from 2 to 1 and measuring voltage between contacts 2 and 3 [24].

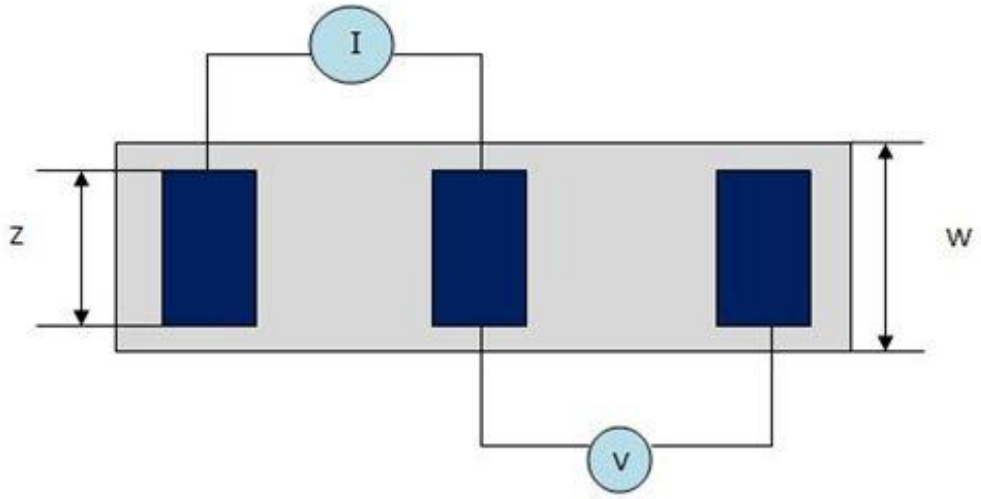

Figure 2.3. Test structure for measuring end resistance measurement by transmission line model

The contact end resistance is thus can be expressed as

$$R_e = (V_{23}/ I) = (R_s * \rho_c)^{1/2} * (1/\sinh(L/L_T)) \quad (2.13)$$

But measuring the end resistance becomes difficult when the contact is very small [30] .This is the limiting factor of the transmission line method.

2.1.4 Transfer length method

Transfer line method was first proposed by Shockley [36] to overcome the inaccuracies of Transmission Line Method. Transfer length method is also abbreviated as TLM but the basic difference transmission line method and transfer line method is that transmission line method is limited to only three contacts whereas transfer line method

allows more than three contacts [30] . The test structure used for the transfer line method is shown in Figure 2.4 as,

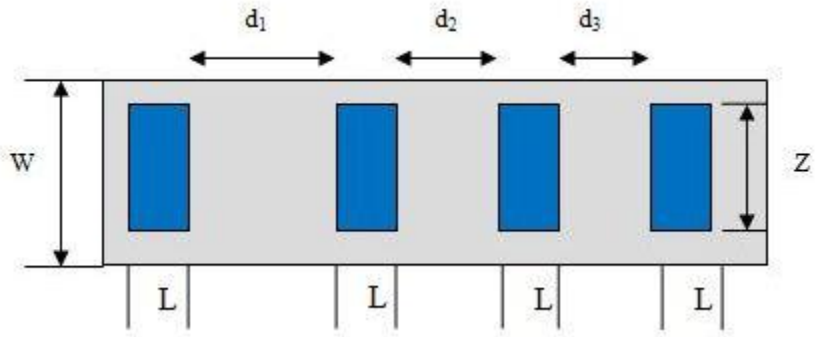

Figure 2.4. Test structure for transfer length method

The total resistance between any two contacts can be expressed as

$$R_T = (R_s * d)/ Z + 2 * R_c \approx (R_s * d)/ Z + (2 * R_s * L_T) / Z \quad (2.14)$$

The value of R_c from equation 2.12 has been substituted in equation 2.14. The total resistance is measured between contact pads for different spacing and plotted against the distances [15] as shown in Figure 2.5. The sheet resistance R_s can be extracted from the slope of the graph. The sheet resistance can be defined as

$$\Delta (R_T) / \Delta (d) = R_s / Z \quad (2.15)$$

where Z is the width of the contact pad. The sheet resistance can be calculated by multiplying the slope to the width of the pad.

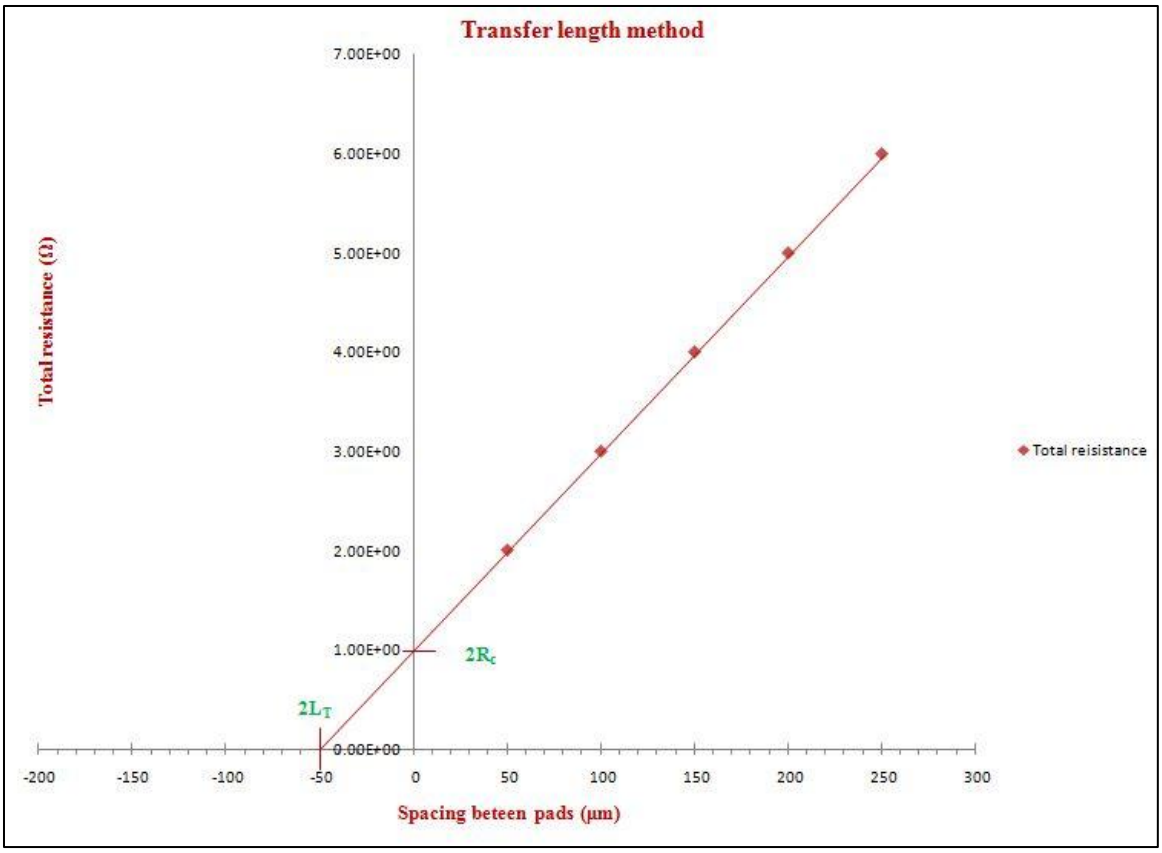

Figure 2.5. Plotting of total resistance against spacing between pads according to transfer length method

The twice of the contact resistance is measured as the total resistance at point d=0. The total resistance thus can be measured as

$$R_T = 2 * R_c \tag{2.16}$$

Again at $R_T = 0$,

$$d=2*L_T \tag{2.17}$$

From equation 2.17, the transfer length can be extracted. The specific contact resistivity (ρ_c) is calculated from the transfer length and sheet resistance. The relationship between transfer length, sheet resistance and specific contact resistivity is given as equation 2.10.

2.1.5 Four point measurement

Four point measurement for metal-semiconductor contact resistance has different resistance parameters. Each probe touching the metal layer has probe resistance (R_p), a probe- to- metal contact resistance (R_{cp}), a semiconductor sheet resistance (R_s) and metal-to-semiconductor contact resistance (R_c). The pictorial presentation of the resistances is shown in Figure 2.6.

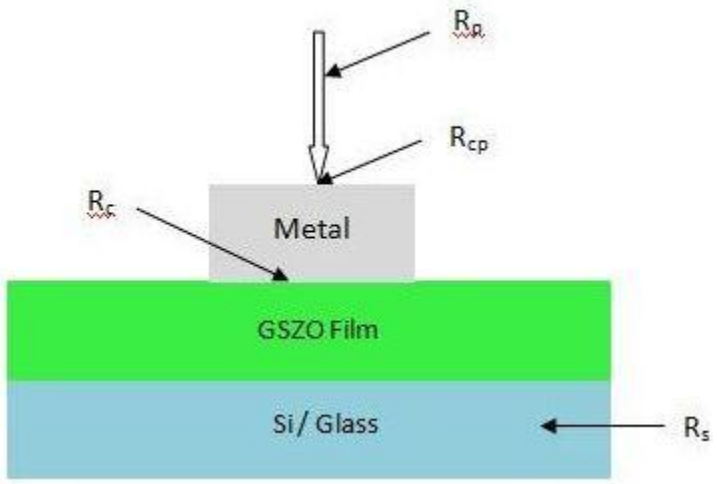

Figure 2.6. Various resistance parameters in four point measurement

Among the four probes, two probes are set on one contact pad and the other two are on another pad. Between the two probes on each contact pad, the outer one is connected to the current source and the inner one to the voltmeter. The four probe connections and the corresponding circuit diagram are shown in Figure 2.7 and 2.8.

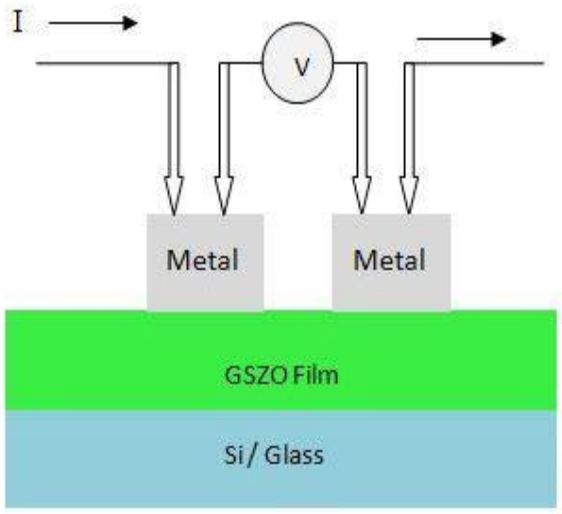

Figure 2.7. Probe set up on the contact pads

The total resistance is calculated from the measured voltage and current using Ohm's law, given as

$$R_T = V / I \tag{2.18}$$

The probe resistances are very small compared to those of voltmeter, so the probe resistances (R_p) and probe to metal resistances (R_{cp}) are negligible with respect to the contact (R_c) and sheet (R_s) resistances. Thus, contact resistance (R_c) and sheet resistance (R_s) contribute to the total resistance.

As all the resistances are in series combination in the circuit arrangement shown in Figure 2.5, the total resistance can be calculated by adding all of them which leads to expression 2.19.

$$R_T = R_{p2} + R_{cp2} + R_c + R_s + R_c = 2* R_c + R_s \tag{2.19}$$

Both equations 2.18 and 2.19 can be combined into one expression (equation 2.20), which relates the contact resistance and sheet resistance with the current passing through the circuit.

$$R_T = 2^* R_c + R_s = V / I \qquad (2.20)$$

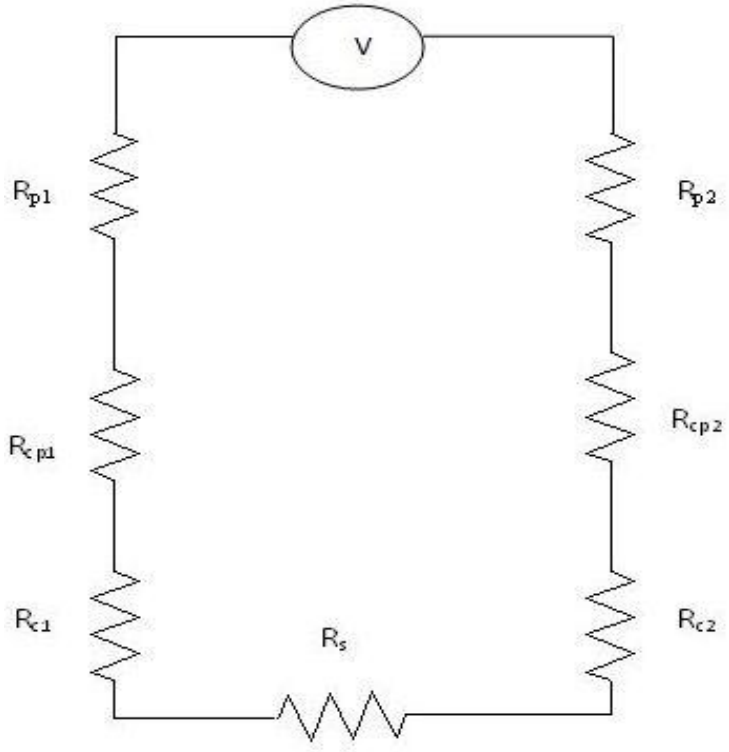

Figure 2.8. Circuit diagram of various resistance parameter of four probe set up

2.2 Study of Electrical Characteristics of Different Contacts

Gong-Ru Lin and S.-C.Wang [37] investigated electrical and structural properties of (002)-oriented high resistivity ZnO films grown on different substrates such as

SiO_2/Si, Si and corning 7059 glass. Al (500 nm) metal contacts were made on the ZnO film with different substrate structures .Transmission line method was used to calculate the specific contact resistivity. For ZnO/Si sample, the contact resistance, sheet resistance and specific contact resistivity were demonstrated as 1.02 x 10^9 Ω, 3.8 x 10^{10}Ω/□ and 1.54 x 10^3 Ωcm^2 respectively. The ZnO/SiO_2/Si sample exhibited the contact resistance, sheet resistance and specific contact resistivity of 8.24 X 10^5 Ω, 1.61 x 10^9 Ω/□ and 2.37 x 10^{-2} Ωcm^2. The contact resistance, sheet resistance and specific contact resistivity of ZnO/Glass sample were found to be as 1.18 x 10^7 Ω, 2.26 x 10^9 Ω/□ and 3.47 cm^2.

Han-Ki Kim et al. [2] reported contact resistance measurements of nonalloyed Al (60 nm) and Al (20 nm)/Pt (50 nm) ohmic contacts deposited on Al doped n-ZnO. The specific contact resistivity was calculated by circular-transmission line method (c-TLM). The specific contact resistivity were considered to be very low for as deposited Al and Al/Pt contacts calculated as 8X10^{-4} and 1.2x10^{-5} Ωcm^2 , respectively. Current-voltage characteristics also showed linear behavior which indicated ohmic contacts.

Han-Ki Kim et al. [4] investigated electrical characteristics of Al (20 nm)/Pt (50 nm) ohmic contacts on Al doped n-ZnO epitaxial layer. Specific contact resistivity and current-voltage characteristics were revealed with respect to different annealing temperatures. The specific contact resistivities for the as-deposited samples were calculated as 1.25 (±0.05) x 10^{-5} Ωcm^2 using circular-transmission line method (c-TLM). The current-voltage data showed ohmic contact (linear trend). The samples were then annealed at different temperatures of 300 ^{o}C and 600 ^{o}C for 1 minute in nitrogen ambient. The best result was achieved for sample annealed at 300^{o}C with less contact resistivity of

2 (±0.25) x 10^{-6} Ωcm^2 and with an improved current-voltage characteristic. The sample annealed at 600^{o}C exhibited specific contact resistivity of 8(±0.3) x 10^{-5} Ωcm$^{2.}$ The current-voltage characteristics were also deteriorated as compared to the samples annealed at 300^{o}C and as- deposited ones.

Han-Ki Kim and Ji-Myon Lee [1] demonstrated electrical properties of nonalloyed Al (50 nm), Al (30 nm)/Au (50 nm) and Al (30 nm)/Pt (50 nm) ohmic contacts. The metal contacts were made on n-type ZnO:Al (2 x 10^{18} cm^{-3}). The contacts had low specific contact resistivity calculated by circular-transmission line method (c-TLM). The specific contact resistivities were calculated for as-deposited Al, Al/Au, Al/Pt as 8.5 x 10^{-4} Ωcm^2, 8 X 10^{-5} Ωcm^2 and 1.2x10^{-5} Ωcm^2, respectively. All the contacts showed linear current-voltage behavior (ohmic contact) and Al/Pt had the best fit as ohmic contact.

Han-Ki Kim et al. [3, 38] presented metallic contact of Ti (30 nm)/ Au (50 nm) on n-type ZnO:Al. The samples were annealed after metal deposition at 300^{o}C and 500^{o}C for 1 minute at nitrogen ambient. The specific contact resistivities found by using circular-transmission line method (c-TLM) were 2 x 10^{-2} Ωcm^2, 2 x 10^{-4} Ωcm^2 and 1 x 10^{-3} Ωcm^2 for the as deposited, 300^{o}C and 500^{o}C contacts, respectively. All of the contacts showed liner current-voltage behavior. The 300^{o}C sample was observed to exhibit higher contact quality compared to the as- deposited and 500^{o}C contacts.

2. 3 Thin Film Transistors Processing

Amorphous oxide semiconductors (AOSs) are better performed candidates compared to all the materials examined till now. Among different AOSs, amorphous GSZO is comparatively low cost material and exhibits improved electrical performance. Hence, amorphous GSZO has been chosen as the material for our thin film transistor. A detailed literature review on the amorphous oxide semiconductors thin film transistors is presented in this section.

Flat- panel displays (FPDs) are of greatest demand in all electronic devices. These have become part of the daily use such as cellular phones, laptop and personal computers. The leading flat- panel display is the active- matrix liquid-crystal display[6]. Basically, displays consist of thousands and millions of matrix pixels. The thin film transistor plays the role of a switch to each pixel to turn it “on” or “off”. In the last few years, amorphous oxide semiconductors (AOS) thin film transistors have been investigated to a great extent for implementation in active-matrix thin film transistors [39] due to their higher electrical performance compared to the conventional semiconductor (Si) and polycrystalline semiconductors [40].These TFTs are expected to have high electron mobility, high on/off current ratio and low threshold voltage for high performance [11]. AOS TFTs have been produced on different substrates like Si [12] and glass [41] . The main advantage of AOS are they possess characteristics of both amorphous and polycrystalline semiconductors. Further, the associated TFTs can be produced at room temperature making them compatible with low temperature processes required for polymeric substrates like plastic [12]. Plastic substrates are of light weight,

flexible , low cost and low power, that makes them suitable for both military and consumer products [6] [9].

Kenji Nomura et al. [7] proposed fabrication of TFTs using amorphous indium gallium zinc oxide (a-IGZO), a transparent amorphous oxide semiconductor. The TFT had a 30 nm thick a-IGZO active layer, 140 nm thick Y_2O_3 as gate insulator and ITO (Sn: 10 %) as the source, drain as well as gate transparent electrodes. The length (L) of the channel was 50 μm and the width (W) being 200 μm. Pulsed laser deposition was used to form the layers and the electrodes. The threshold voltage of the TFTs was measured 1.6 V which indicates the enhancement operating mode. The on-to-off current ratio was ~ 10^3.

Hitaso Yabuta et al. [41] fabricated TFTs with channel of a-IGZO rf-magnetron sputtering at room temperature with a field- effect mobility of 12 $cm^2V^{-1}s^{-1}$, an on-off current ratio of ~10^8, and a sub threshold gate voltage swing of 0.2 $Vdecade^{-1}$. The channel layer of material a-IGZO film had a controlled conductivity from about 10^{-3} to 10^{-6} S cm^{-1}. To control the conductivity of the film, the sputtering gases, O_2 / (O_2+Ar) mixing ratio was varied form ~3.1% to 3.7%. The TFTs were n-type and operated in enhancement mode. The TFTs productions were performed on the unheated Corning 1737 glass substrate onto which the 50-nm-thick a-IGZO film was deposited. On top of the a-IGZO layer, 140-nm- thick Y_2O_3 was deposited acting as gate insulators. The highest temperature observed in the chamber after the deposition of the channel layer and insulators were 40^o C and 140 ^{o}C, respectively that are below the temperature commercially used for plastics films used in the electronic devices. The TFTs made had a

L of 10 μm and W of 150 μm. The TFTs were patterned by photolithography and lift off process. All the electrodes were Au (40 nm)/Ti(5 nm) structures formed by electron beam evaporation. Fortunato et al. [11] demonstrated fabrication of TFTs produced by rf-magnetron sputtering at room temperature. The thin film transistors were fabricated using non conventional oxides like amorphous Indium-Zinc-Oxide (IZO) semiconductor. The channel layer (15 nm) as well as the source and drain region electrodes (100 nm) were fabricated using the Indium-Zinc-Oxide by rf (13.56 MHz) magnetron sputtering from a ceramic target of Super Conductor Materials. The deposition pressure was 0.15 Pa. The O_2 / Ar flow ratios were 0.15 and 0.02, the power densities were 5 and 9 W/cm^2 for the active channel layer and source/drain electrodes, respectively. Borosilicate glass of 1 mm thickness was used as the substrate onto which the channel layer was deposited. The channel layer was then coated with a 200 nm sputtered ITO film which acted as gate electrode and a 200 nm atomic layer deposition ATO film acted as dielectric. The channel length was 57 μm and width-to-length ratio being 35. The thin film transistor pattering was done by lift-off process. The TFTs thus produced operated in the enhancement mode with threshold voltage of 2.4 V. The TFTs had high electron mobility of 22.7 cm^2 / Vs, gate voltage swing of 0.44 V/dec and an on/off current ratio of 7X10^7.

Later Fortunato et al. [12] reported two series of high mobility In free amorphous oxide TFTs. Sn was used as substitution for In. For one series, a-GSZO film was deposited at the room temperature and for the other series; the film was deposited at 150^o C. A 50 nm thick a-GSZO film layer was deposited using rf magnetron co-sputtering using 3 in. diameter ZnO: Ga_2O_3 ceramic targets and 2 in. diameter Sn target in super

conductor crucibles were used at 15 cm from the substrate. The base pressure of the co-sputtering was $3X10^{-4}$ Pa, an oxygen partial pressure of $1X10^{-1}$ Pa, a processing pressure of (Ar + O_2) of 7 $X10^{-1}$ Pa and rf power of 75 and 20 W for the ZnO:Ga_2O_3 and Sn targets, respectively. P-type silicon substrate was used to produce the TFTs coated with 100 nm thick thermally grown SiO_2 to use as gate dielectric. Si was used both as the substrate and the common gate of the device. To act as gate electrode, a (5/75 nm) thick (Ti / Au) film was deposited by electron-beam evaporation on the backside of Si. A 50 nm thick a-GSZO layer was then deposited and 200 nm thick source/drain electrodes (Ti) were electron-beam evaporated on top of a-GSZO. Lift-off process was used to pattern both the semiconductor and the source/drain layers. Both series of transistors had a fixed width (W) of 50 nm and length (L) of 50 nm. After production, both series of TFTs were annealed in nitrogen, at 150 °C, 200 °C, 250 °C, and 300 °C for 1h using the Barnstead Thermolyne F21130 tubular furnace. The produced TFTs had high saturation mobility of 24.6 cm^2/V s, a sub threshold gate swing voltage of 0.38 V/decade, a turn-on voltage of −0.5 V, a threshold voltage of 4.6 V, and an I_{on}/ I_{off} ratio of $8x10^7$.

CHAPTER 3

EXPERIMENTAL DETAILS

3.1 Contact Resistance Measurement by Transfer Length Method

The goal of this work is to measure the contact resistance of different metals on GSZO films. These films were deposited over the oxide layer (SiO_2) that is thermally grown on the substrate of Si. The experimental part includes photolithography process, metal deposition, resistance measurements by four probe method and the determination of current-voltage relationship.

3.2 Lithography Process

3.2.1 Basic photoresist types and materials parameters

Photoresists (PR) are basically classified as two types, positive and negative photoresist. The exposed areas of the photoresist layers are soluble or insoluble to the solvent (developer) based on the photoresist types. The photoresist is applied to the thin film deposited on a substrate, usually, Si or SiO_2, and then exposed to the ultraviolet light through a mask. The mask has clear and obscure aspects that determine the desired pattern to be created on the photoresist layer. In case of positive photoresist, the exposed region is soluble to the developer and a positive image of mask is created on the resist. But for negative photoresist, the unexposed area gets dissolved in the developer solution. The photoresist region that remains after the development protects the other layers of the sample during the following steps. The component materials of the photoresist are matrix

material or resin, photoactive compound (PAC) and solvent [42]. The resin provides the adhesion of the photoresist layer to the substrate. The resin is not chemically active to the irradiation. Resin gives the resist the mechanical properties like thickness, etch resistance, flexibility and thermal flow stability. The role of solvent is to keep the resist in liquid form until the processing is done. The photoactive compound is the active ingredient of the photoresist. The photoactive compound is responsive to the radiation and goes under chemical reaction when exposed to the ultraviolet ray. These photochemical changes occur due to the radiant energy [42].

3.2.1.1 Positive optical photoresist

Positive photoresist is considered to be more demanding because of the high resolution capability that supports exposure from 0.5 μm to 2 μm for semiconductor device fabrication. The resist can be exposed for both g-line (436 nm) and i-line (365 nm) ultraviolet ray [42] . The matrix component of positive photoresist is novolac resin [42] which provides the adhesion of the resist layer to the underlying substrate. The novolac resin is soluble to aqueous base. Diazonaphthoquinones [42] is utilized as the photoactive compounds in positive photoresist. Diazonaphthoquinones is not soluble to aqueous base like developer and prevents the resin being dissolved into the developer. Photoactive compounds work as inhibitor here to the unexposed area in case of positive photoresist. The photoactive compounds decrease the dissolving rate of the unexposed area when the development is done. A positive image is thus created from the mask onto the substrate which is shown in Figure 3.2. Propylene-glycol-monomethyl ether (PGME) [42] is used as the solvent in the positive PR.

3.2.1.2 Negative optical photoresist

Among the three components of negative photoresist, cyclized rubber resin is used as the matrix component which is highly soluble in non-polar organic solvents (tolune and xyline). Bis-arylazide is used as photoactive compound in the negative photoresist. Negative photoresist has less resolution capabilities than positive resist which makes unsuitable for critical dimension 2 μm and 3μm [42]. But better adhesion to substrate and lower cost are provided by negative photoresist. For negative photoresist, the exposed region becomes less soluble in the developer solvent. A cross linked three dimensional molecular network is produced in the photochemical reaction which makes the irradiated portion insoluble. When photoresist coated sample is exposed to the ultraviolet light, the arylazide gets excited and nitrogen is produced from the photochemical reaction. Then nitrene is formed by the nitrogen which is considered as an extremely reactive intermediate compound which takes part in the different subsequent chemical reaction and generates molecules [42]. As a result, the photoresist in the unexposed region get dissolved but in exposed area remains unchanged. The pattern formed after applying negative photoresist is shown in Figure 3.1. Post exposure baking must be done in between the exposure and development of the wafer. Otherwise, the whole photoresist gets dissolves in the developer solvent and no pattern is formed.

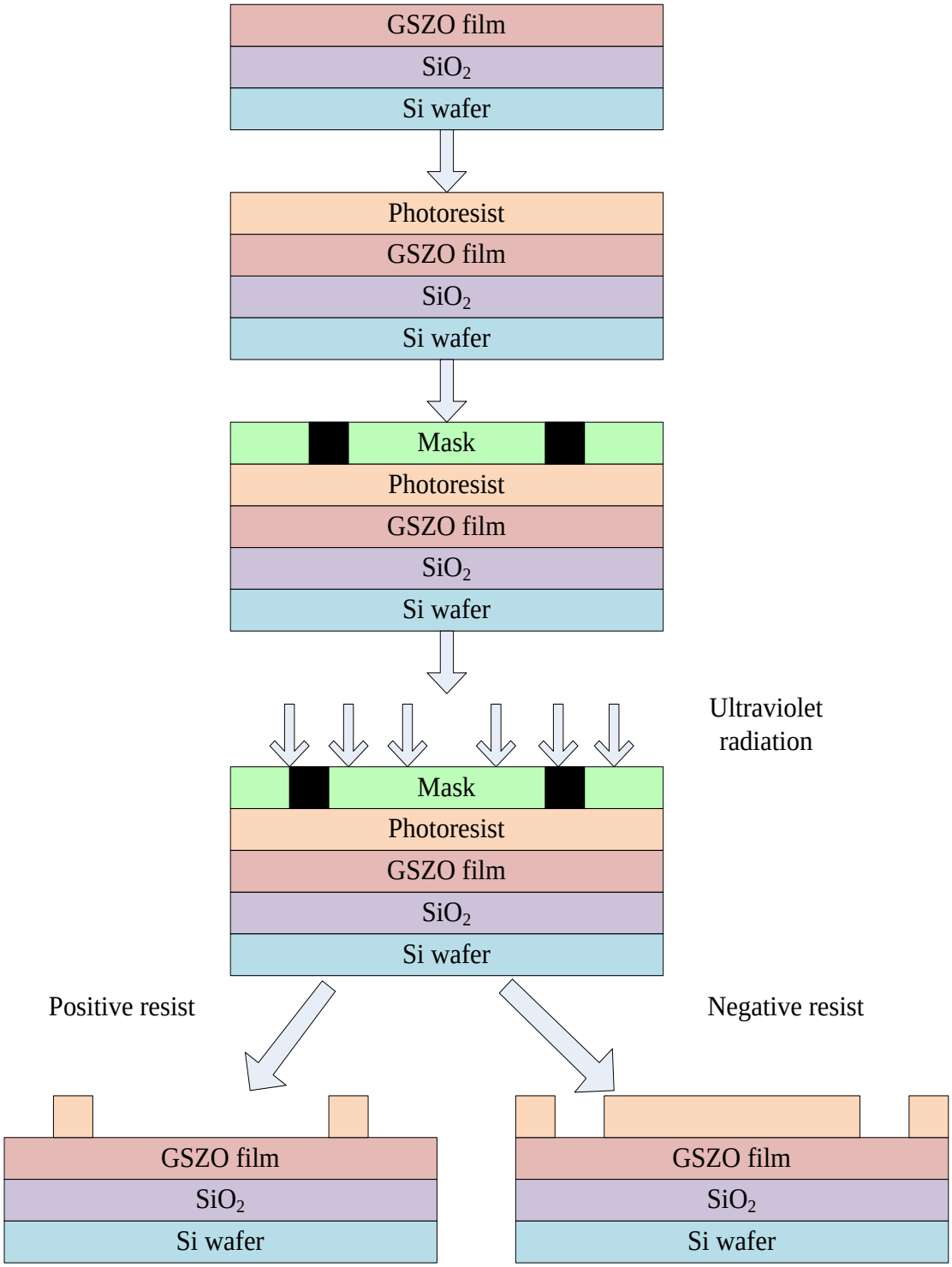

Figure 3.1. The resulting patterns developed after positive and negative photoresist applications

3.2.2 Sample cleaning

Defect is caused by different types of contaminants like particulates, films and also residues from chemicals used at different stages of thin film transistor fabrication [42]. These contaminants can be sourced from equipments used in the processing, chemicals, water, chemical bottles even from the personnel working in the lab and moisturizer from the atmosphere. Cleaning the wafers properly is therefore very important to make the devices perform better. Poor adhesion is caused by contaminants between the photoresist and the underlying layers of the substrate. Ultrapure chemicals and deionized water are used during processing [38]. The wafers are usually wet after being cleaned with chemicals and rinsed with water. If the photoresist is applied on the wet surface, poor adhesion is made between the resist and the other layers of the sample. Water is attracted by the hydrophilic elements (oxides); but repelled by hydrophobic photoresist. Moisture is thus taken by oxides from the air. The photoresist layer thus gets dehydrated. The dehydrated resist has low adhesion quality. Baking of the cleaned wet sample is done to reduce the moisture and improves the adhesion quality.

The sample is cut to the desired size, which varies according to application and is submerged into the 500 mL of trichloroethylene for 1 minute with ultrasonic bath to remove particulate material from the surface as well as any existence of metallic impurities. The sample is then cleaned with acetone and propanol in the same way in sequence [38]. The sample is rinsed with deionized water. The sample is blown with nitrogen and heated for 1 minute to ensure the good photoresist adhesion.

3.2.3 Priming

The wafer is primed with an adhesion increaser material before the photoresist coating. After cleaning and baking, the wafer is coated with adhesion promoter. Hexamethyldisilazane (HDMS) [42] is used as the adhesion promoter. The coating is done by the spinner to make a uniformly thick layer over the wafer. The cleaned and dried wafer is placed on a flat and hollow metal chuck. The metal chuck is connected to the vacuum and has some small holes at the center. These holes hold the wafer down tightly by the vacuum so the wafer does not move away from the holder while spinning. The adhesion increaser (HDMS) is then applied on the sample using a clean syringe and spun it at 3000 rpm for 30 seconds. The amount of the HDMS taken was determined according to the sample size. HDMS provides good adhesion to the photo-resist and the GSZO film surfaces. HDMS functions by removing the OH groups from the surface. HDMS first undergoes reaction with water on the surface and generates NH_3, oxygen and an inert (HDMS) that produce hydrated surface. More HDMS (during soft baking) then takes part in reaction with oxygen which produces trimethylsilyl ($Si[CH_3]_3$) [42]. Trimethylsilyl acts as binder between the photoresist and surface. Trimethylsilyl continues reaction and a water repelling photoresist layer with low surface energy is formed. It was then heated (soft baking) on a hot plate for one minute to remove any moisturizer. The sample is then set back on the spinner chuck for the negative photo-resist application. Figure 3.2 shows the spinner and the sample holder that has been used for the coating of the samples.

(a)

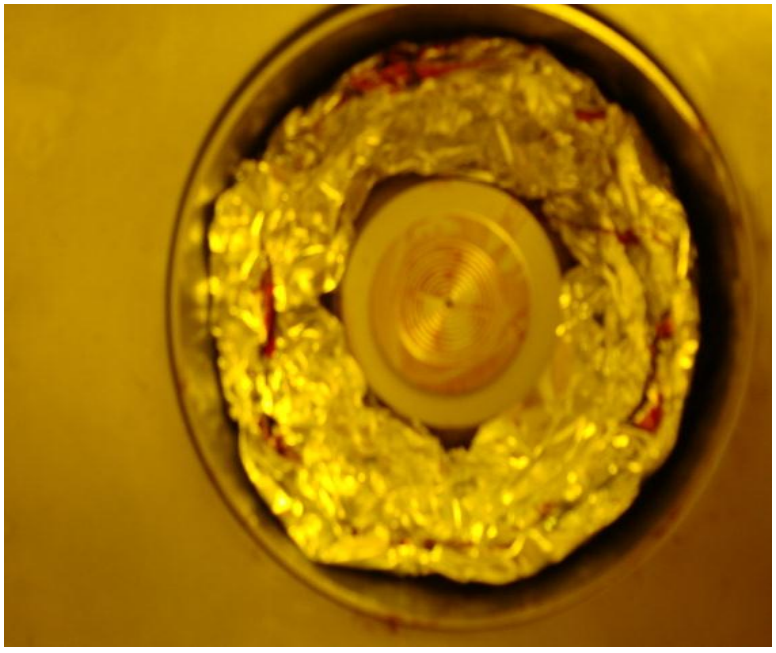

(b)

Figure 3.2. (a) The spinner and (b) the sample holder.

3.2.4 Negative photo-resist application

After cleaning, baking and priming, the wafer is coated with negative photoresist. The photoresist is released on the wafer and spun at the same speed for 30 seconds.

3.2.5 Soft baking

Soft baking should be done right after the wafers are coated with photoresist. Soft baking is considered to be a very important step in the processing as the parameters of the subsequent steps like exposure and developing times are dependent on the soft baking conditions. Soft baking reduces the level of solvent in the resist that convert the liquid film cast into solid form which reduces contamination of particulates. The amount of solvent contained in the photoresist gets reduced after spinning and soft baking. But, the rate of attack of the photoresist layer by the developer is dependent on the residual solvent concentration. The high residual solvent concentration in the resist after soft baking increases the dissolution rate. The residual solvent concentration of the resist can be controlled by the soft baking parameters (baking time and temperature). The film layer gets stressed due to the force during spinning .The layers thus gets separated and adhesion becomes poor. The stress is released and adhesion is improved by the softbaking.

Excessive reduction of the solvent by the soft baking can make the photoresist layer very thin. This ultra thin layer is not sufficient to protect enough during the etching process. Again if the soft baking is done for a long period of time, the entire photoactive compound undergoes the chemical reaction and the photosensitivity is reduced.

Among all the soft baking equipments (hot plate, convection and infrared oven), hot plate is considered to be the standard one for providing greater control over temperature and consistent dispersal of the heat. Hot plate is used to heat the wafer in our work. Soft baking is carried out in air for 1 minute at the temperature of 90^{o} C.

3.2.6 Exposure

The coated wafer is placed on the sample holder of QUINTEL Q-2001CT wafer aligner system and the mask is set on the wafer facing off. The "EXPOSURE" button is turned on to expose the sample in the ultraviolet ray. The wafer is exposed for 30 seconds and then the exposure is turned off.

3.2.7 Post exposure baking (PEB)

Post exposure baking is done to reduce the ridges in the resist sidewall profile by diffusing the photoactive compound in the resist, from the unexposed region to the exposed region of the wafer. The photoactive compound in the resist of the exposed region goes into the reaction that causes reduction of photoactive compound in this area and so photoproduct is produced. On the other hand, no chemical reaction happens in the unexposed portion of the wafer that makes this area to contain photoactive compound. When the post exposure baking is done, diffusion of photoactive compound happens through the resist from the unexposed area to the exposed area which creates an average effect across the boundary.

Post exposure baking (PEB) is done to complete the reaction initiated during the exposure. A post exposure baking performed near the softening point of the photo resist reduces mechanical stress formed during soft bake and exposure of especially thick resist

films due to the expanding nitrogen and therefore improves resist adhesion. However, a certain delay between exposure and post exposure baking is required to outgas N_2. Otherwise, during PEB the N_2 in the resist will expand and increase mechanical stress in the film [4]. For this system, the post exposure baking is done for 1 minute on a hot plate.

3.2.8 Pattern development

The primary function of the development process is to convert the resist latent image created in the exposure process into the real one which acts as the mask in the next steps (etching). The unexposed region of the film is also attacked by the developer and the film thickness is reduced. The condition for a standard and successful developer is that the dissolving rate should be different for the exposed and unexposed regions. But the attack rate of the unexposed region should be nominal. The developer should be selected in such a way that the developing time should be short enough to produce perfect output image without much thinning of the resist. The wafer should undergo through the rinsing just after the exposure because the developing does not stop until this is completely removed from the developer. For the development process, 500 mL of negative photo-resist developer is taken in the beaker and the wafer is immersed into the developer for 30 seconds. The wafer is then rinsed with water and blown with nitrogen gas to get it dried.

3.3 Plasma Cleaning

Plasma cleaning is intended to remove the contaminants from the surface layer of the wafer. The contaminant can be from different sources, such as chemical or natural.

The sample is developed in the chemicals and then rinsed with the water. The contaminants are thus mostly organics. The plasma cleaning process is done before the metal deposition to improve the adhesion to the metal of the surface by removing the organic materials.

Surface cleaning is a multi-step process consisting of generation of active (cleaning) species, their transport to the surface ,the reaction on the surface and the ultimate removal of the reaction products from the surface [43].

Plasma cleaner MODEL PC2000 is used for plasma cleaning. A vacuum pump of system with base pressure of 200 millitorr is connected to the system. The typical operating pressure is in the 50-200 millitorr range. The chamber has outer diameter and height of 8 inch and 4 inch, respectively, as shown in Figure 3.3(b). A power supply of 150 watts and 13.56 MHz frequency is used for the cleaning process. The chamber is vented to load the sample. The sample is mounted on to the 6 inch diameter stainless steel sample holder inside the chamber which is also presented in Figure 3.3 (b). The pump button, shown in Figure 3.3 (a) is turned on to reduce the pressure of the chamber. When the pump pressure is decreased down from 999 millitorr to close to 0, “GAS 1” switch is turned on to let the oxygen gas enter into the chamber. The water connection should also be turned on to cool down the system. The time period of 5 minutes is set in the timer and the RF forward power to 150W. As operating pressure should be 50 millitorr, when the pump pressure starts going down, the pressure to adjusted to 50 millitor. The “RF” power switch is turned on. If the color of the oxygen plasma is not shown, the chamber is pumped again to get proper vacuum. The pumping process is repeatedly done until the

color is turned to white. The sufficiency of oxygen plasma in the chamber is indicated by the change of the color. The plasma cleaning is done for 5 minutes. After the plasma cleaning is done, the contact angles are measured to indicate the degree of the smoothness of the surface.

(a)

(b)

Figure 3.3. (a) Plasma cleaner MODEL PC2000 (b) the vacuum chamber and sample older

3.4 Metal Deposition

Electron beam evaporation is used to deposit various contact making metals on the film. An elaborative description of the electron beam evaporation is presented later in the section 3.8.

3.5 Lift-Off Process

Lift off is the process to strip the metal from the wafer where the photo-resist exists. Acetone and propanol are used for the lift off process. A 100 mL of acetone is taken in a glass beaker and the sample is submerged into the acetone. The beaker is placed in the ultrasonic bath for three minutes. The metal layer gets removed. The sample is inundated into the propanol for 1 minute and the beaker is agitated with hand. Even after cleaning with acetone and propanol, sometimes the metal particles stay on the sample. *N*-Methyl-2-pyrrolidone (NMP) is very effective to remove the metal particle. The sample is put into the 100 mL NMP and cleaned with ultrasonic for 3 minutes. The remaining particle gets removed from the sample. The sample is then rinsed with deionized water and blown dry with nitrogen gas.

3.6 Resistance Measurement by Four Probe Method

Four probe method is used to measure the total resistance between the contact pads. Three different patterns of electrodes have been used for the transfer length method measurements. Each pattern is designed with a set of contact pads of the same size and different spacing between them. The contact pad sizes used for this work are 1 x

$1mm^2$, 500 x 500 μm^2 and 300 x 300 μm^2. Four different probes of same radius are used in the four probe system. The probes are set on the two adjacent pads locating two probes on each pad. The probes on each contact pad are arranged in such a way that one probe is near to the inside edge and the other one is close the outside edge. The pictorial description of the probes set up is shown in the Figure 3.4. The inner two probes are connected to the voltmeter and outer two probes are connected to the current source. Each probe is placed on a base which has a magnet to attach the probe firmly with the surface. The sample is mounted on the sample holder. The Keithley 236 source measurement unit has been used to pass the current of about 1 μA through the contacts and the corresponding voltage drop is displayed on the voltmeter screen. The voltage measured is the voltage drop between the two contacts. The measurements of the voltage drop of rest of the pads are performed in the same way. The total resistance is achieved by dividing the voltage with the current.

3.7 Current-Voltage Characteristics

The current-voltage (I-V) characteristics data have been measured by the Keithley Interactive Test Environment semiconductor parameter analyzer (SPA). The characterization has been done for different annealing conditions. The variations in the behavior of the contacts with increased annealing duration have been determined. Two probes are situated on the two different contact pads. the voltage of range -1 V to +1 V have been set to get the corresponding current passed through the contacts and spacing between them.

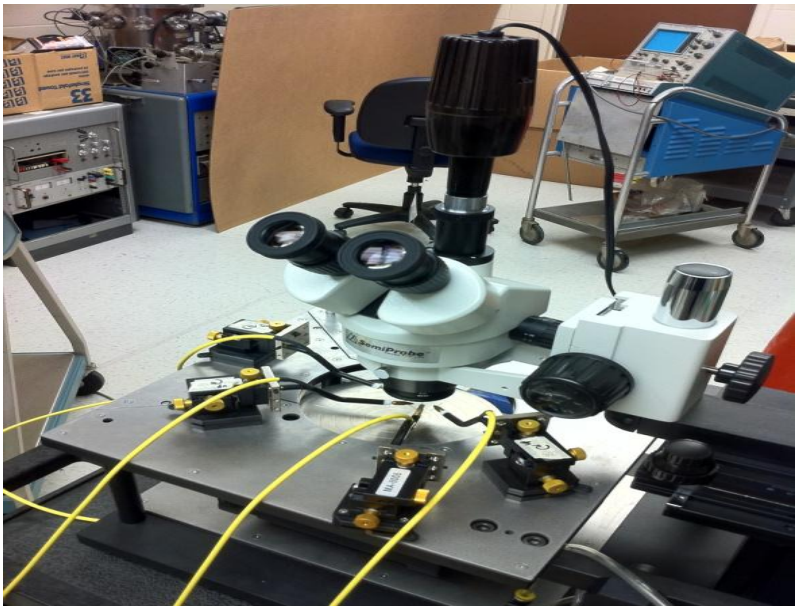

Figure 3.4. Four probe set up

3.8 An Overview of TFT Processing

As TFTs are produced over a supporting substrate, single crystal Si is used as substrate in TFT fabrication. SiO_2 of thickness 122.5 nm is utilized as a dielectric layer. A GSZO thin film layer of approximate thickness of 33 nm has been deposited on top of the SiO_2 layer. All the samples are annealed in air at 250^o C for 1 hour. The steps of the TFT fabrication are shown in order in the form of flow chart in Figure 3.5.

Removal of contaminants from the wafer is imperative in TFT processing. Particulate can create abnormalities in the resist coating that could negatively affect the performance of the TFTs. The fabrication is initiated with the cleaning of the sample and is maintained throughout the process. The sample is then coated with photo-resist. For our TFTs, each sample is coated twice; initially with positive photo-resist and later on with negative photo-resist. Since photoresist is a light sensitive material, all the steps of

the photolithography process are done in yellow room where the ultraviolet fluorescents are filtered to prevent unwanted exposure. First, the positive photoresist application is performed on the sample. Soft baking is done on coated wafers to remove the solvents from the surface of the sample. The wafers are then exposed and developed to get the intended pattern. Etching is exhibited to remove the unwanted film .Stripping is done to remove the photoresist from the unexposed region of the sample. The wafer again undergoes the coating of the HDMS and negative photoresist, respectively. The softbaking is performed after each coating. The coated wafer is aligned by the mask aligner with respect to the previous pattern and the mask. The wafer is baked after exposure and developed with the solvent subsequently to get the pattern of the TFT. Wet ability of the sample is improved by the plasma cleaning. Metals are then deposited on the sample to make the contacts. Electron beam evaporation technology is used to deposit metals of desired thicknesses. The lift-off process is then exhibited to remove the metal from all over the sample but the contact areas. The metal should only remain on the surface where the photoresist is chemically removed by the stripping method. Detailed discussions on the steps of photolithography such as sample cleaning, priming, negative photoresist coating, manual exposure, post exposure baking, soft baking and pattern development for negative photoresist have been presented in the earlier sections (Sect. 3.2.2 -3.2.8). Soft baking and lift-off processes are also described in sections 3.3 and 3.5, respectively. Positive photoresist application, pattern development, wafer alignment, stripping, etching process and metal deposition by electron beam evaporation are reviewed in the following sections.

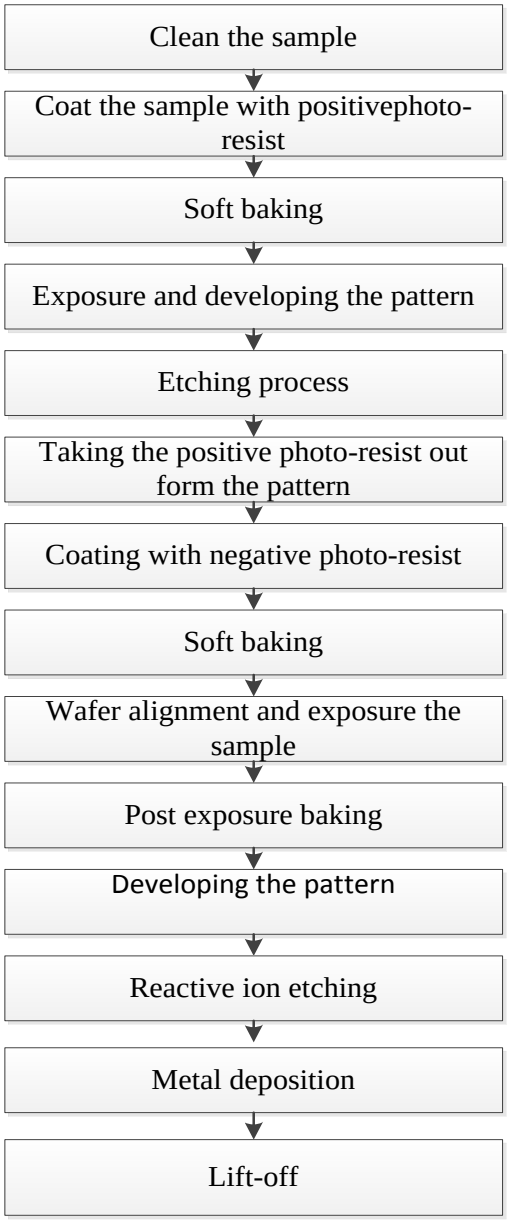

Figure 3.5. The steps of thin film transistor fabrication

3.9 Positive Photoresist Application

The process of positive photoresist application is similar to that of negative photoresist. The sample is spinned at 3000 rotations per minute for the duration of 1 minute. Soft baking is done after the application of positive photoresist. The sample is

then exposed to the ultraviolet ray using the QUINTEL Q-2001CT Wafer Aligner system.

3.9.1 Wafer alignment system

The QUINTEL Q-2001CT wafer aligner system is used to transfer the pattern from the mask to the surface of the wafer. An image of QUINTEL Q-2001CT wafer aligner system is shown in Figure 3.6. An power supply of 200 W is connected to the system to turn the light on. The arc light need around current and voltage of 5 A and 50 V, respectively. The nitrogen valve has to be opened to ensure the gas flow to cool down the lamp

The first step of loading the mask involves lifting the optical head. An air compressor air valve in used to operate the optical head up and down. This valve is identified as in the figure 3.6. The vacuum pump with a valve is used, which is connected to the mask holder and needs to be opened. The mask is placed on the mask holder as shown in Figure 3.7 with the metal side facing down and the MASK CLAMP switch is activated to get the vacuum. The vacuum area of the mask holder is covered by the wafer. The MASK LOAD switch is turned on which locks the mask on the holder properly. Optical turret position ROW AND COLUMN VIEW is utilized to observe the wafer and the position of the wafer with respect to the mask can be determined by carrying out the microscope scan. The wafer is aligned with respect to the mask using a coarse alignment knob.

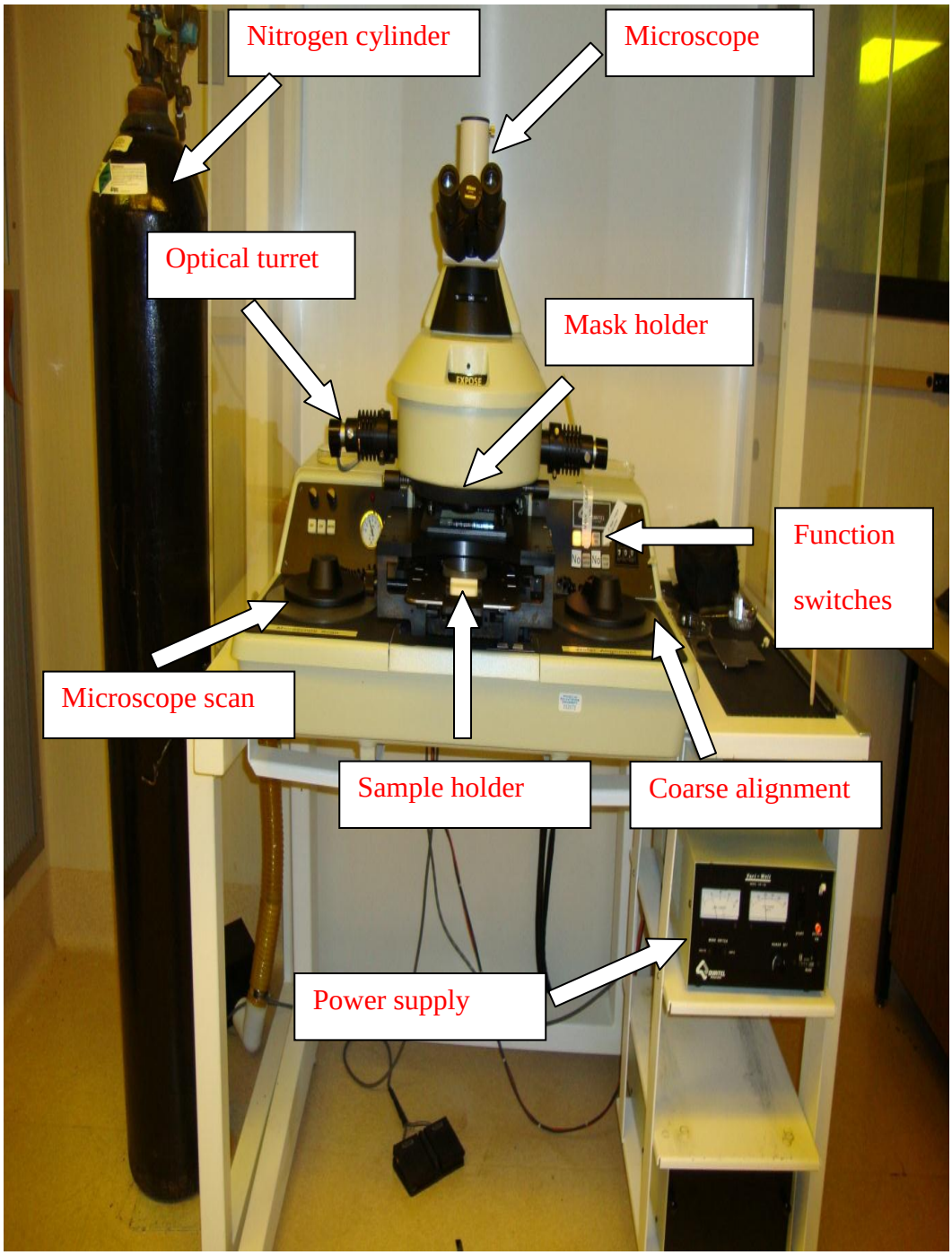

Figure 3.6. A QUINTEL Q-2001CT wafer aligner system

To load the sample, the sample holder tray is pulled out to deactivate the vacuum. The wafer is loaded onto the vacuum chuck facing the coated surface up and the flat part directed to the operator. The tray is pushed slowly inwards until the CHUCK VACUUM switch gets activated. The WAFER LOAD switch is then activated. The Air-Bearing Guide is set to raise the sample holder that makes contact between the wafer and the mask in separation mode. A close view of the sample holder is in Figure 3.8.

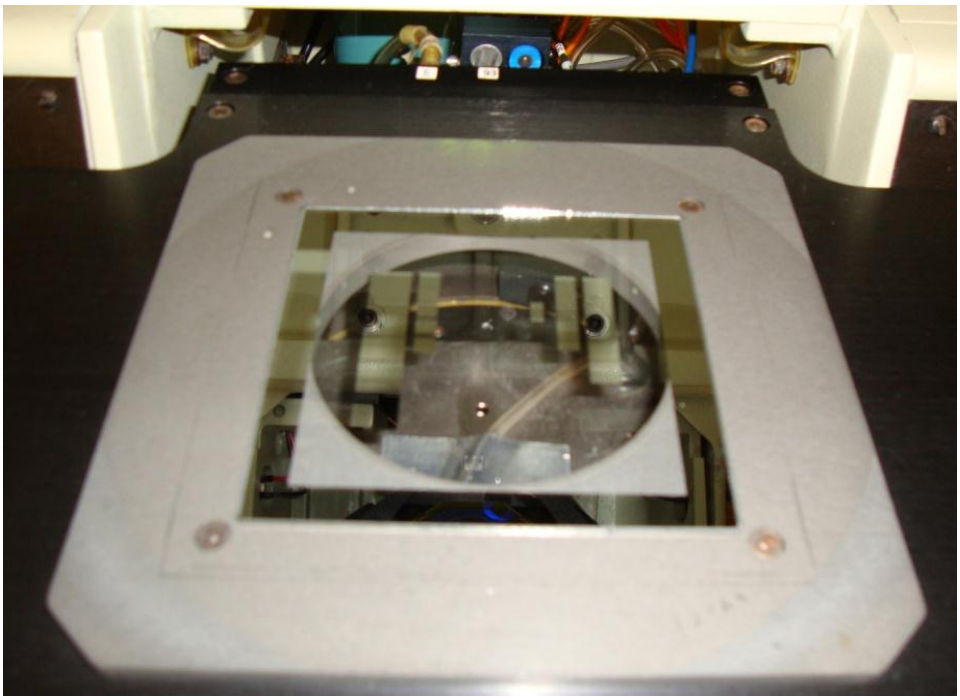

Figure 3.7. Mask holder

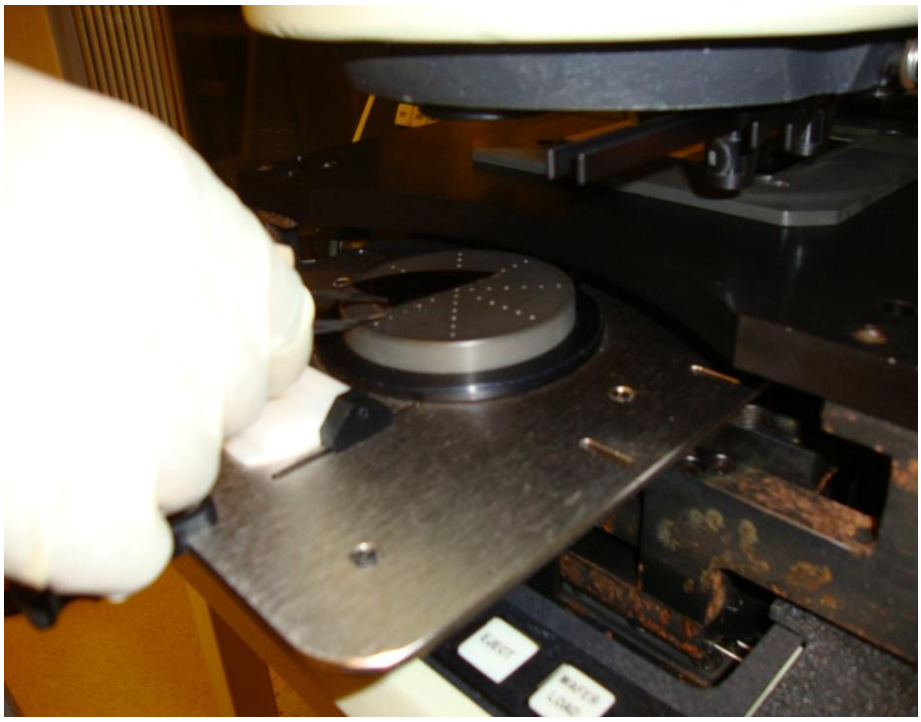

Figure 3.8. Sample holder

With the optical turret in the Split Field Adjustment Microscopic position, the wafer location with respect to the mask is checked whether the mask is placed properly onto wafer so that the pattern is placed in the intended position. If the pattern is not on the right position, the WAFER ROTATION CONTROLS are used to rotate the wafer clockwise or counterclockwise and the COARSE ALIGNMENT to control the movement of the sample in the X-Y direction.

3. 9.2 Exposure of the sample

After the soft baking, the wafer is ready for expose to the ultraviolet light. An energy integrator is used to measure the total energy impinging on a unit area of the sample. Thus the degree of exposure is controlled by operating the amount of energy. The goal of the exposure is to create the latent image of the pattern from the mask.

When the alignment is done properly, the sample and the mask should be in contact mode to get exposed. If the wafer is not in contact mode, the shutter does not get opened. The optical turret should be set to expose mode. The time is set to 30 seconds. The SHUTTER button is pressed to start the exposure. The sample is exposed to the ultraviolet ray of wavelength for 30 seconds. The power supply setting for the lamp has a voltage of 220 volts and current of 5 amperes. When the exposure is complete, the shutter gets closed automatically and the sample holder is released and comes down automatically. The tray is pulled out slowly and the sample is removed from the sample holder. The sample is ready for developing.

3.9.3 Pattern developments

Positive photo-resist developer is taken in a beaker and diluted with deionized water to a 1:1 ratio. The sample has been placed into the developer for 1 minute. The sample is taken out and rinsed the sample with deionized water for 1 minute. The pattern is developed on the surface of the sample. To dry the sample, the sample is blown dry with the nitrogen gas. The pattern produced after development is shown Figure 3.9.

3.10 Etching The Barrier Layer

Chemical etching is used to remove the GSZO film layer and SiO_2 barrier that are not protected by the photo-resist. The ratio of chemical used for the etching process is 0.1 mL of HCL acid and 100 mL of deionized water. The acid is added to the water in a glass beaker. The sample is placed into the mixture for 15 seconds.

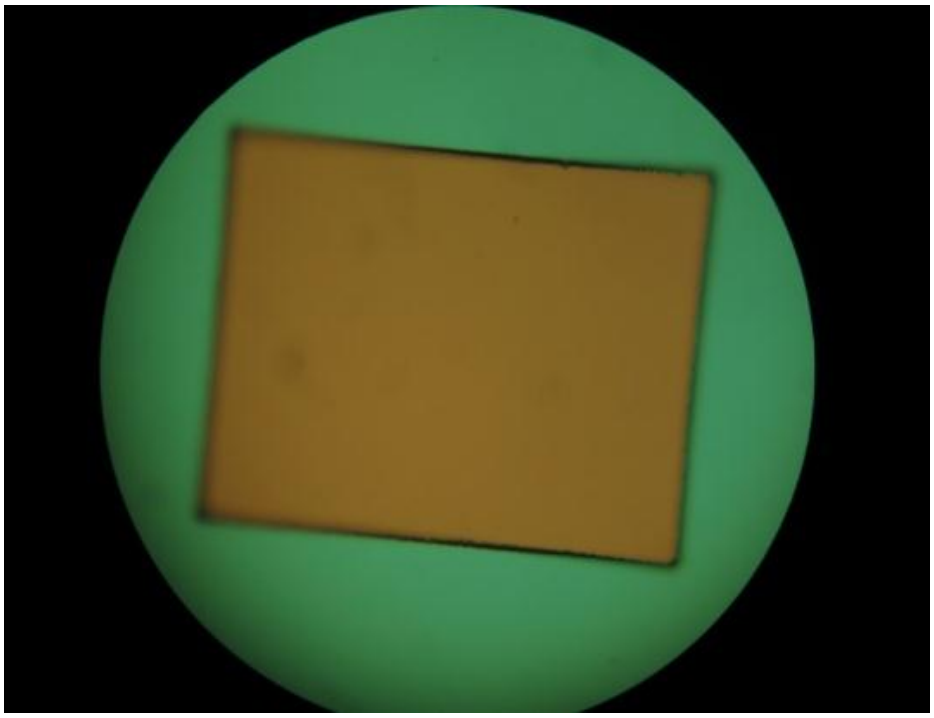

Figure 3.9. Pattern developed after positive photo-resist application

The chemical ratio and the etching time are very critical for a successful etching process. If the sample is over etched, then the barrier and film layer even under the photo resist of the pattern gets removed leaving only the bare Si wafer.

3.11 Removal of Positive Photo-resist

Acetone and propanol are used to remove the photo-resist. The sample is submerged into 100 mL of acetone and put it into the ultrasonic bath for at least 3 minutes. After the photo-resist is removed, the sample is placed into the 100 mL of propanol for 2 minutes. Then the sample is rinsed with the deionized water and blown dry with nitrogen. After removal of the positive resist, negative photoresist coating is done on

the etched sample. The pattern developed from positive photoresist application is aligned with respect to the design in the mask.

3.12 Alignment of The Sample

The mask is loaded on the sample holder properly followed by the sample. The loading procedure is mentioned in the earlier section (Mask Alignment).With the optical turret in the Split Field Adjustment Microscopic position, the position of the sample with respect to the mask has been checked to see whether the mask on the sample is placed properly so that the wings (source and drain) falls on the right position onto the square. If the wings are not on the right position, the WAFER ROTATION CONTROLS are used to rotate the wafer clockwise or counterclockwise and the COARSE ALIGNMENT to control the movement of the sample in the X-Y direction. Alignment is done very carefully because if the alignment is not proper, components of the transistors are not set in the appropriate place and the structure becomes incorrect. The sample is exposed to the ultraviolet ray for 30 seconds. The sample is then baked and submerged into the negative photo-resist developer for 30 seconds. The sample is rinsed with deionized water and blown with nitrogen gas to dry after the development. The patterned wafer is baked at 90^{o} for 1 minute for removing the water remained after rinsing with water. Figure 3.10 shows the structure of the TFT after the photo lithography process. The pattern achieved after photolithography process is examined with the microscope to ensure the proper structured pattern to deposit the metal. The dimension of the pattern is sometimes

deteriorated if the parameters of the photolithography process are not determined appropriately.

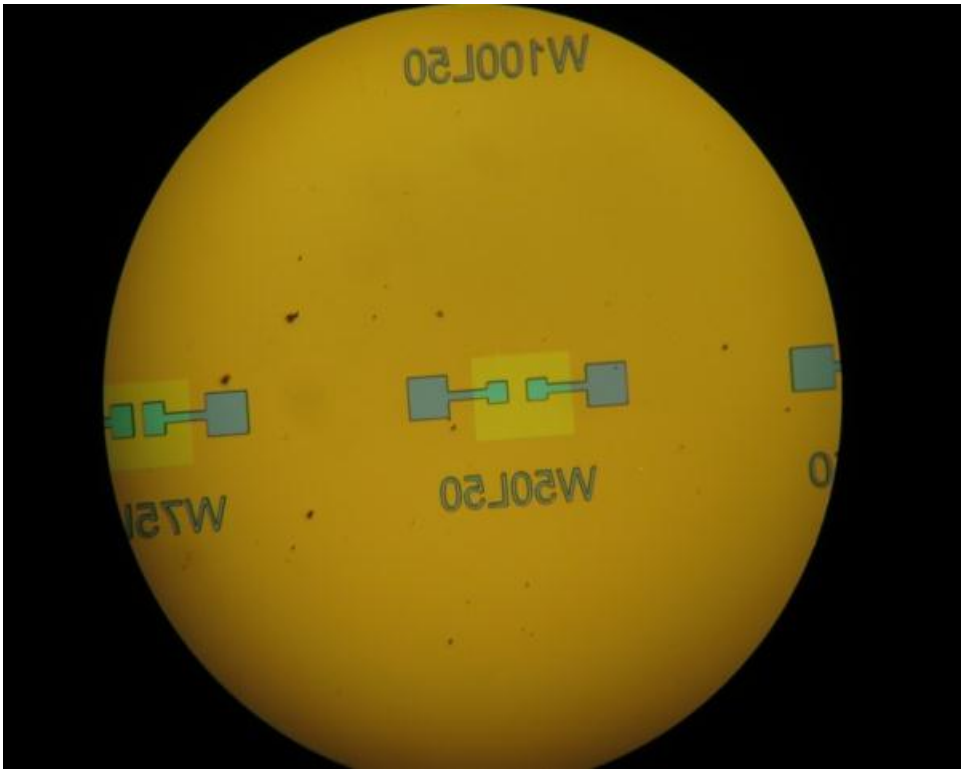

Figure 3.10. Thin film transistor after the photolithography process

3.13 Metal Deposition

Electron beam evaporation is used to deposit the metal (Ti and Au) to make the contact. Electron beam evaporation ensures wide range of control over the evaporation system. Thus the thickness and deposition rate are maintained easily by electron beam evaporation. Sequential depositions of more than one material are allowed during the evaporation by electron beam evaporation. Since sequential depositions of Ti and Au are required to be done, the use of the electron beam evaporation system becomes essential.

3.14 Introduction to Electron Beam Evaporation

Electron beam evaporation is achieved by electron bombardment. Electron stream is accelerated with high energy 5 to 10 KV and focused onto the evaporant surface in the crucible. The direction of electron stream is controlled by the magnetic field. When the electrons impinge onto the evaporant material, most of the kinetic energy is converted into the heat. The temperature is really high, approximately 3000^{o}C. The evaporant material gets evaporated and the vapor is directly driven to the target object (substrate). The whole process needs to be done inside the vacuum chamber where extremely low pressure is maintained. Filaments are used to produce the electrons. One of them is located inside the ion gauge controller. The gas inside the ion gauge controller gets ionized. When the vapor is reached onto the substrate, they are condensed back to the solid state. Depositions from multiple sources are possible as the evaporated materials are located in different crucibles. Better uniformity is achieved because of the large mean free path, big chamber and high vacuum. The basic working principle of electron beam evaporation is shown in figure 3.11. By electron beam evaporation, the pressure inside the chamber can reach upto 10^{-6} or higher. This high pressure makes the chamber contaminants free to a great extent to improve the contact quality of the metal and the surface.

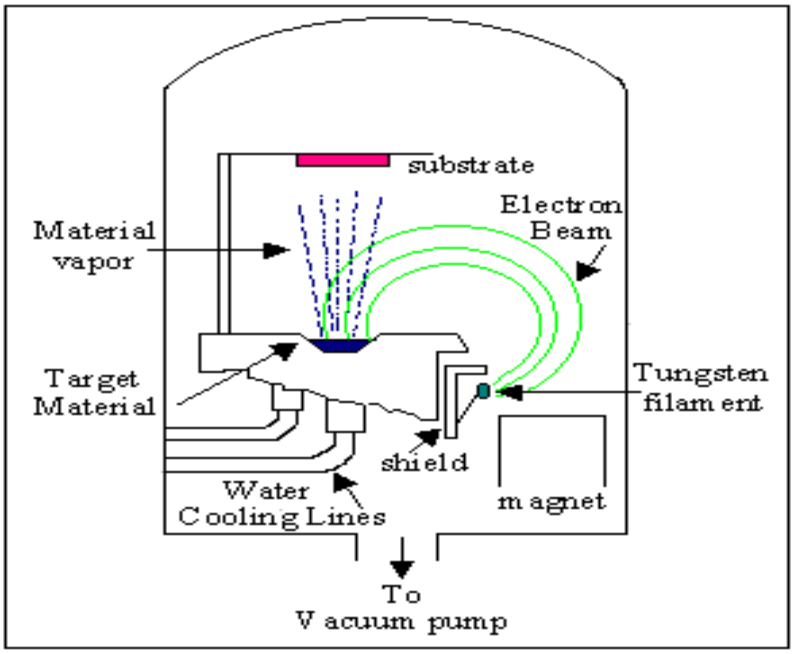

Figure 3.11. Pictorial description of working principle of electron beam evaporation process [44]

3.15 KJL 4500 Ionization Gauge Controller

The ionization gauge controller only works when the pressure inside the chamber reached to a certain pressure level. The ion gauge tube must be turned on when a good vacuum is achieved (9.9 X 10^{-4} or higher). The pressure is shown on the display. The power specification for this controller is 185 watts. The ion gauge is made up of two KJL-600 thermocouple tubes. The thermocouple tubes are used to measure the pressure with range 1 to 1 X 10^{-3} Torr. An ion gauge of type Bayard-Alpert with range 9.9 X 10^{-4} to 1.0 x 10^{-10} Torr is inserted to convert the gas to the ion. The emission current is adjustable 1.0 mA to 20 mA. Figure 3.12 (a) shows the picture of KJL 4500 Ionization Gauge controller and the ion gauge.

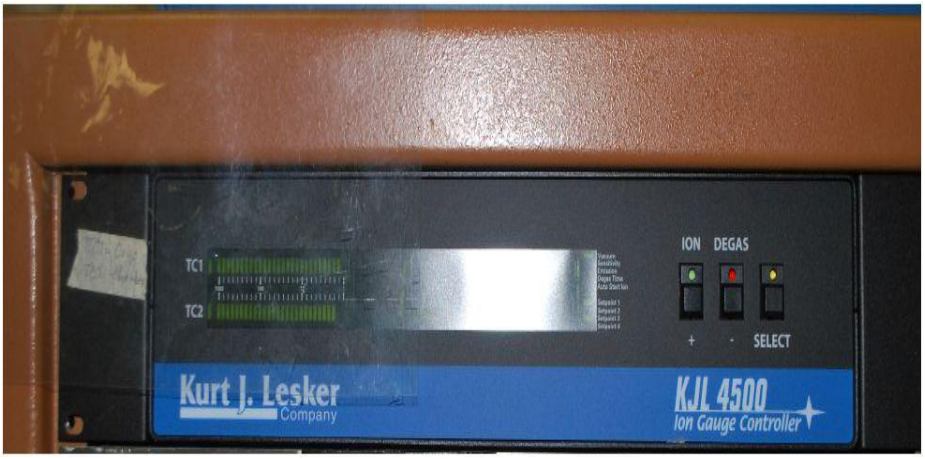

(a)

(b)

Figure 3.12. (a) KJL 4500 ionization gauge controller and (b) ion gauge

Between the two thermocouples, thermocouple 1 is used in monitoring the vacuum system pressure and displaying the pressure on a bar graph located on the front panel of the controller. Thermocouple1 is also displayed when the ion gauge is off and the vacuum pressure is not achieved. The thermocouple 2 is used to measure the pressure of the roughing pump.

The basic operating principle of ionization gauge is to ionize the gas presented in the gauge and to collect the gas ions. A current flow to the ion collector circuit is caused by the positively charged ion. The pressure of ion gauge is measured from the magnitude of current. If the pressure of gas molecules is more, then ionization rate is also high and this causes a high amount of current flow to the collector circuit. The ion gauge is enclosed in a glass. The ion collector is a slender wire down the center of a grid structure which is shown in Figure 3.12 (b). Two electron emitting tungsten filaments are located outside the grid structure. Power is supplied to the filament. The filament gets heated and electrons are emitted in high vacuum pressure range. The emitting current is usually a few mA. The emitted electrons are accelerated to the grid. The accelerating potential difference is 150 volts.

3.16 Procedure

3.16.1 Sample loading into the chamber

The chamber is vented to load the wafer. The Nitrogen gas flow is turned on. The chamber gets opened due to the nitrogen gas pressure. The sample holder is taken out. The sample is placed at the center of the sample holder and the holder pins are screwed

properly so that the sample does not fall when the holder is flipped. Now the sample holder is set back in the chamber and the chamber lid is closed. The mechanical pump and rough line is now turned on. Remaining air, nitrogen gas and other gases are removed from the chamber by the mechanical pump and lower pressure is achieved inside the chamber. When the pressure on TC2 bargraph display is down close to 10, the rough line, mechanical pump are turned off and the high vacuum is opened.

3.16.2 Setting the deposition profile

The ion gauge controller is turned on when the pressure reaches 10^{-6} or higher. Three hours are commonly required to get the pressure. A thickness monitor is used to set the deposition profile. The thickness monitor is turned on. If "FAIL" appears on the display, the stop button is pushed inside and held for few minutes. Now the thickness endpoint key is pressed. The thickness is shown on the display. The thickness is set by pressing the "up" and "down" keys.. Material impedance and material density are also set in the same way as the material thickness. If a sequence of material depositions is done, then after each deposition a new set up of deposition parameters is required. For our system, a sequential deposition of Ti and Au is done. First, thickness endpoint of Ti (20 nm), material impedance (14.06) and material density (4.5) are set to perform the deposition. After completing the deposition of Ti, again the parameters for Au are to be set to perform deposition. The thickness endpoint, material impedance and material density set for Au are 100 nm, 23.18 and 19.3, respectively.

3.16.3 Deposition

The main circuit breaker should be turned on and wait 5 minutes to get it warm. The “High Voltage” button is now turned on. The voltage gets adjusted to 9 kV. “GUN WATER” button is turned on to cool down the crucible of the evaporant material. The “GUN SHUTTER” is set to auto position. Emission control is placed at zero before starting the deposition. The “GUN FILAMENT” button is pressed and the deposition gets started. The focus is adjusted on the evaporant material by moving “BEAM POSITION” knob and the current is controlled by the “EMISSION CONTROL”. The emission current is shown on the display. When the evaporant material is focused properly, the deposition rate goes high. The required deposition rate for Ti is 1 Å /seconds and Au is 5 Å /seconds. When the thickness endpoint is achieved, the deposition is terminated automatically. The current depends on the amount of material presented in the crucible. Emission control is done carefully, as passing more current can create more heat that may destroy the crucible and hence alignment gets interrupted too.

After the metal deposition, the metal is removed by lift-off process and blown by nitrogen gas. The characterization can now be performed on the fabricated TFT.

CHAPTER 4

RESULTS AND DISCUSSION

4.1 Transfer Length Measurements for Different Metal Contacts

Transfer length method has been applied on different metallization scheme to measure the contact resistances. Effects of different annealing duration conditions (time and ambient) on Al, Au/Al/Ti, Al/Au and Al/Pt contacts have been investigated.

4.1.1 Specific contact resistivity calculation of Al (100 nm) contact on Gallium Tin Zinc Oxide (GSZO) film

Contact resistance, sheet resistance and specific contact resistivity calculation results with respect to different annealing duration have been presented in this section.

4.1.1.1 Contact pad size of 300 micron x 300 micron

Voltage drop between the contact pads for different spacing have been measured by four probe method. Total resistances have been measured by dividing the voltage drop by the current passed through the contacts. The diagram of total resistances vs. spacing between pads for as deposited sample is shown in Figure 4.1. For the as deposited samples, the total resistance values are very high (9.4×10^6-9.6×10^6 Ω). According to the transfer length method, a linear relationship is established between the total resistance, sheet resistance and the contact resistance (Equation 2.14). Hence, a trend line of the total resistances has been drawn. The trend line is then extrapolated. The extended trend line intersects the y-axis at a point which is twice of the contact resistance. The point where the line cuts the x-axis indicates twice of the transfer length. The contact

resistance is calculated as 0.5 x 10^7 Ω. The transfer length is 4.7 x 10^3 μm and the slope found from the plot is 1053.6 Ω/cm. The sheet resistance is extracted from the slope multiplying by the width of the contact pad. The sheet resistance is thus 3.2 x 10^4 Ω/□. The specific contact resistivity results as 7 x 10^3.

The sample is then annealed for 10 minutes in nitrogen ambient. Figure 4.1 illustrates the total resistances values with respect to the distances between pads. The total resistances values (9.17 x 10^6 - 9.27 x 10^6) are not significantly changed from those of as deposited state to affect the sheet resistance. The contact resistance is improved for this post deposition annealing duration. The contact resistance is 4.5 x 10^6 Ω. The transfer length is calculated as 5.5 x 10^3 μm. The sheet resistance and specific contact resistivity are 2.5 x 10^5 and 7 x 10^4Ω-cm^2, respectively. Another post deposition annealing of duration 15 minutes is done on the same sample. The total resistances values are decreased by approximately 5 x 10^6 Ω. The trend line of the total resistances data points intersects the Y-axis at the point of 1 x 10^7Ω and negative x-axis at 3.2 x 10^3 μm shown in Figure 4.1. The contact resistance is thus 1.5 X 10^6 Ω. The transfer length is thus found as 1.6 x 10^3 μm. The specific contact resistivity, sheet resistivity are calculated as 7.3 x 10^2 Ω cm^2 and 2.8 x 10^7 Ω / □ respectively.

A comparison of the values of specific contact resistivity with respect to annealing duration is presented in Figure 4.2. The contact of 300 x 300 μm^2 has the same contact resistivity for as deposited and 10 minutes post deposition annealing duration. The least contact resistivity is observed for the 10+15 minutes. The specific contact resistivity is reducing with the increase of post deposition annealing duration.

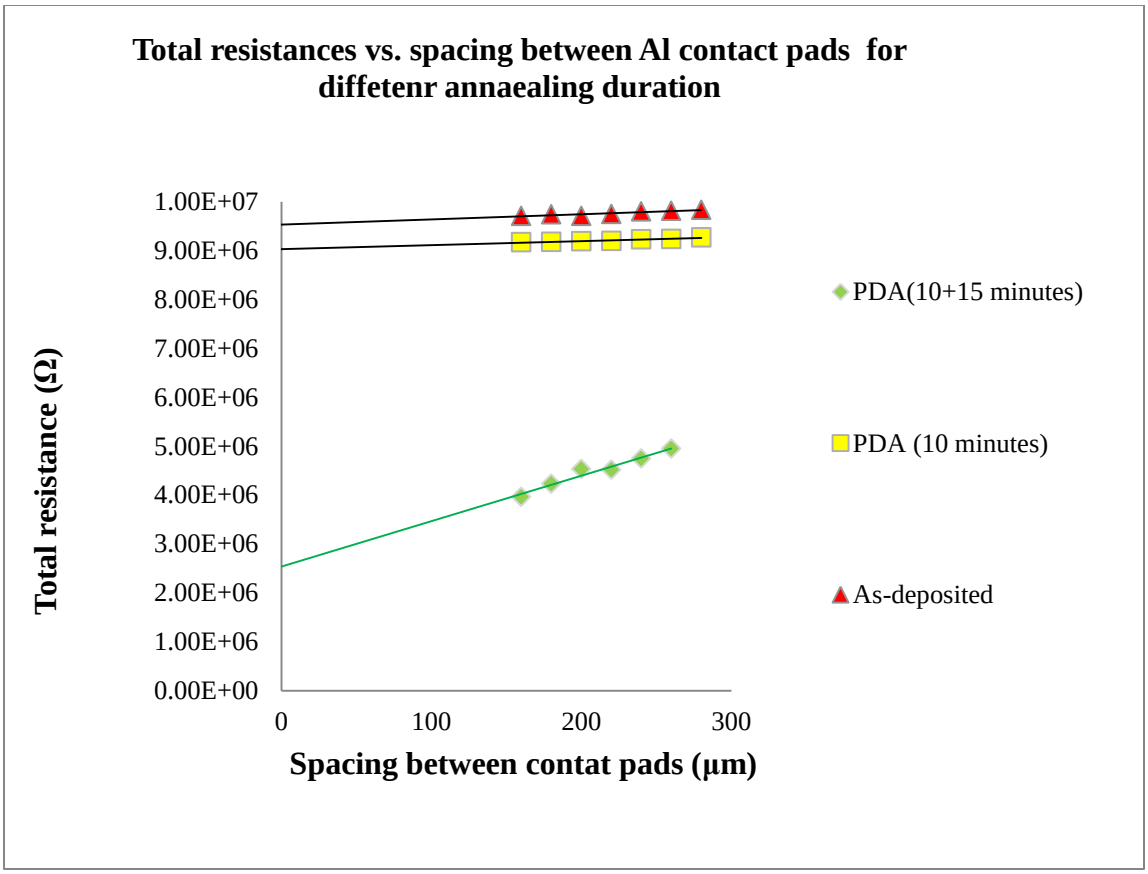

Figure 4.1.– Comparisons of total resistances vs. spacing between contact pads (300 x 300 µm^2) of Al contact scheme for different annealing duration

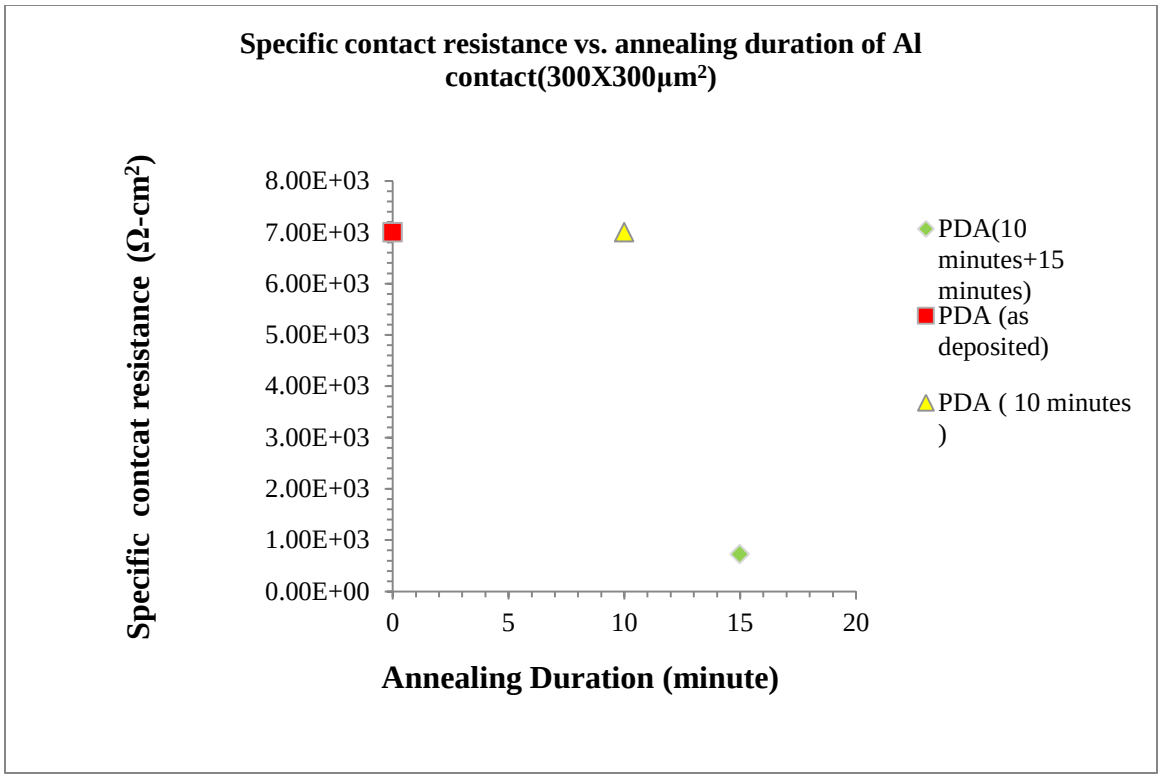

Figure 4.2. Specific contact resistance vs. annealing duration for Al contact (300 x 300µm^2) on GSZO film

4.1.1.2 Contact pad size of 500 micron X 500 micron

The total résistance vs. spacing between contact pads of the as-deposited sample is shown in Figure 4.3.The total resistances values (9.86 x 10^6 Ω to 9.93 x 10^6 Ω) are very high which leads to large transfer length of 1.4 x 10^4 µm. The contact, sheet and specific contact resistances are calculated as 5 x 10^6 Ω, 1.7 x 10^5 Ω/□ and 3.6 x10^5 Ω/ cm^2.

After performing the post deposition annealing for 10 minutes in nitrogen ambient, the contact resistance value calculated from total resistance goes down to 2.5 x

10^6. The transfer length found in the plot (Figure 4.3) is 1.4 x 10^4 μm. The values of 3.2 x 10^6Ω and 4.9 x 10^3 Ω-cm^2 are the sheet and contact resistivity respectively.

The sample is annealed again for 15 minutes in nitrogen ambient to decrease the resistance. The transfer length, contact resistance, sheet resistance and specific contact resistivity are calculated as 50 μm, 3.4 x 10^5 Ω, 3.3 x 10^6 Ω, and 84 Ω-cm^2.The total resistances vs. spacing for different annealing duration are summarized in Figure 4.3. A comparison of specific contact resistances with respect to different annealing durations is shown in Figure 4.4. The specific contact resistivity is reduced with the increased annealing duration.

4.1.1.3 Contact pad size of 1000 micron x 1000 micron

The total resistances (7 x 10^6 Ω – 9 x 10^6 Ω) for as deposited Al contact plotted against spacing between contact pads in Figure 4.5 shows that the contact resistance is too high to pass any current through the device.

The sample is annealed after metal deposition for 10 minutes in nitrogen ambient. The transfer length calculated from the extrapolated trend line is 2.9 x 10^3 μm (Figure 4.5). The contact resistance, sheet resistance and specific contact resistivity are calculated as 4 x 10^6 Ω, 1.4 x 10^6 Ω and 1.1 x 10^5 Ω-cm^2.

The sample is then annealed again for 15 minutes in the same ambient. The plot of total resistance vs. spacing is shown in Figure 4.5.The contact resistance (5 x 10^5 Ω) and transfer length (2.3 x 10^2μm) is decreased than the previous annealing duration. The specific contact resistivity and sheet resistance are calculated as 1.1 x 10^3 Ω-cm^2 and 2.2 x 10^6 Ω, respectively.

A comparison between the specific contact resistivity for different annealing condition is shown in Figure 4.6. This contact is non-conducting for the as deposited sample. The resistance goes down with the increased annealing duration.

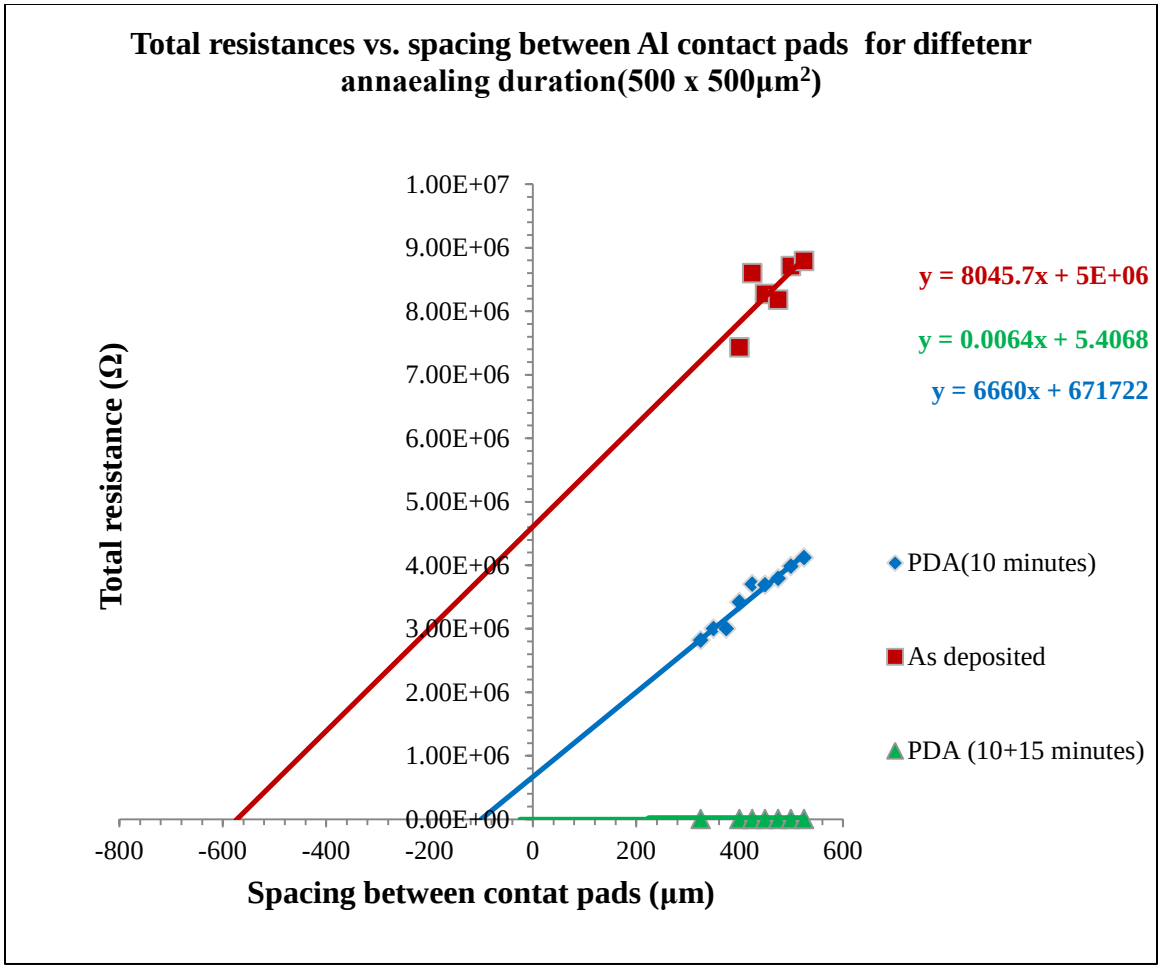

Figure 4.3 Comparisons of total resistances vs. spacing between contact pads (500 x 500 µm²) of Al contact for different annealing duration

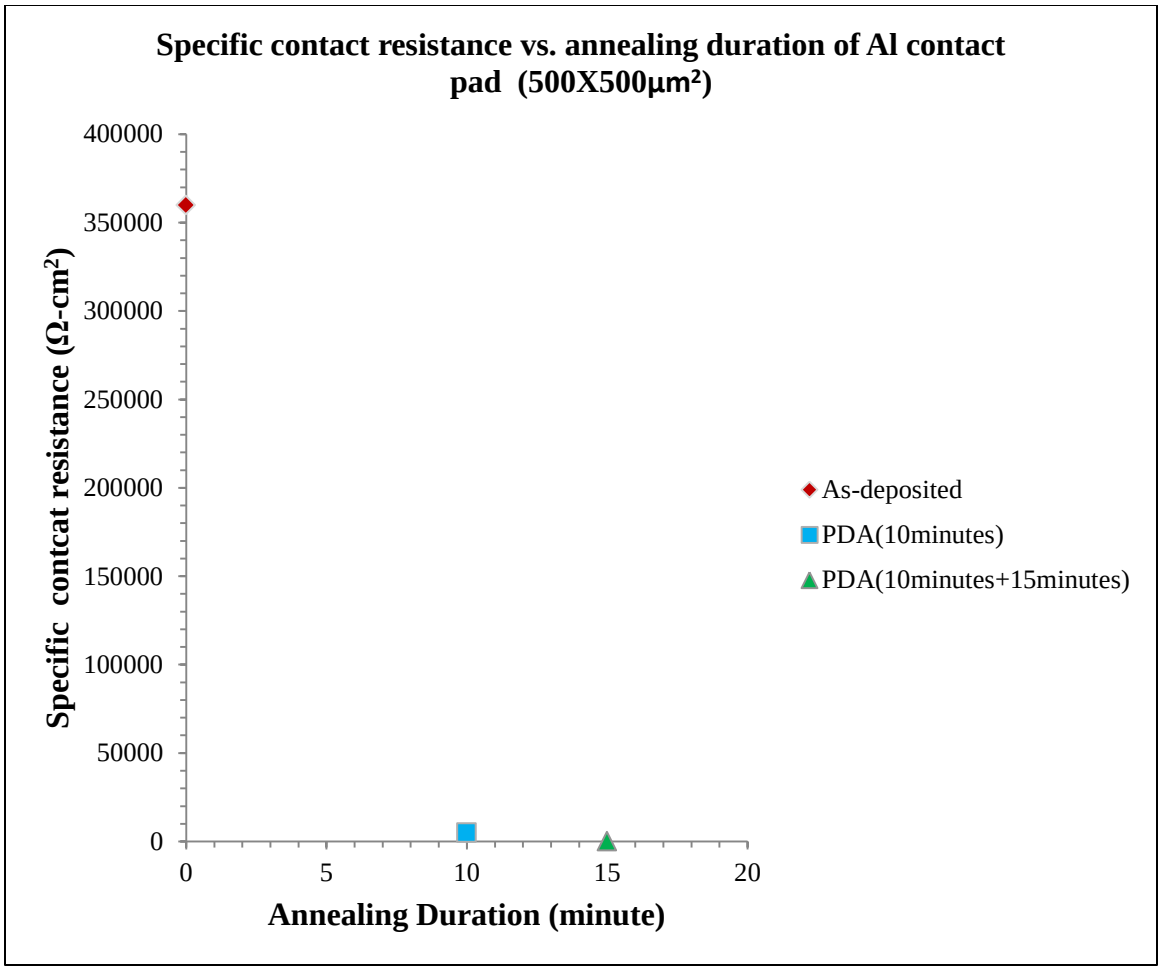

Figure 4.4. Specific contact resistance vs. annealing duration for Al (500 x 500µm^2) contact on GSZO film

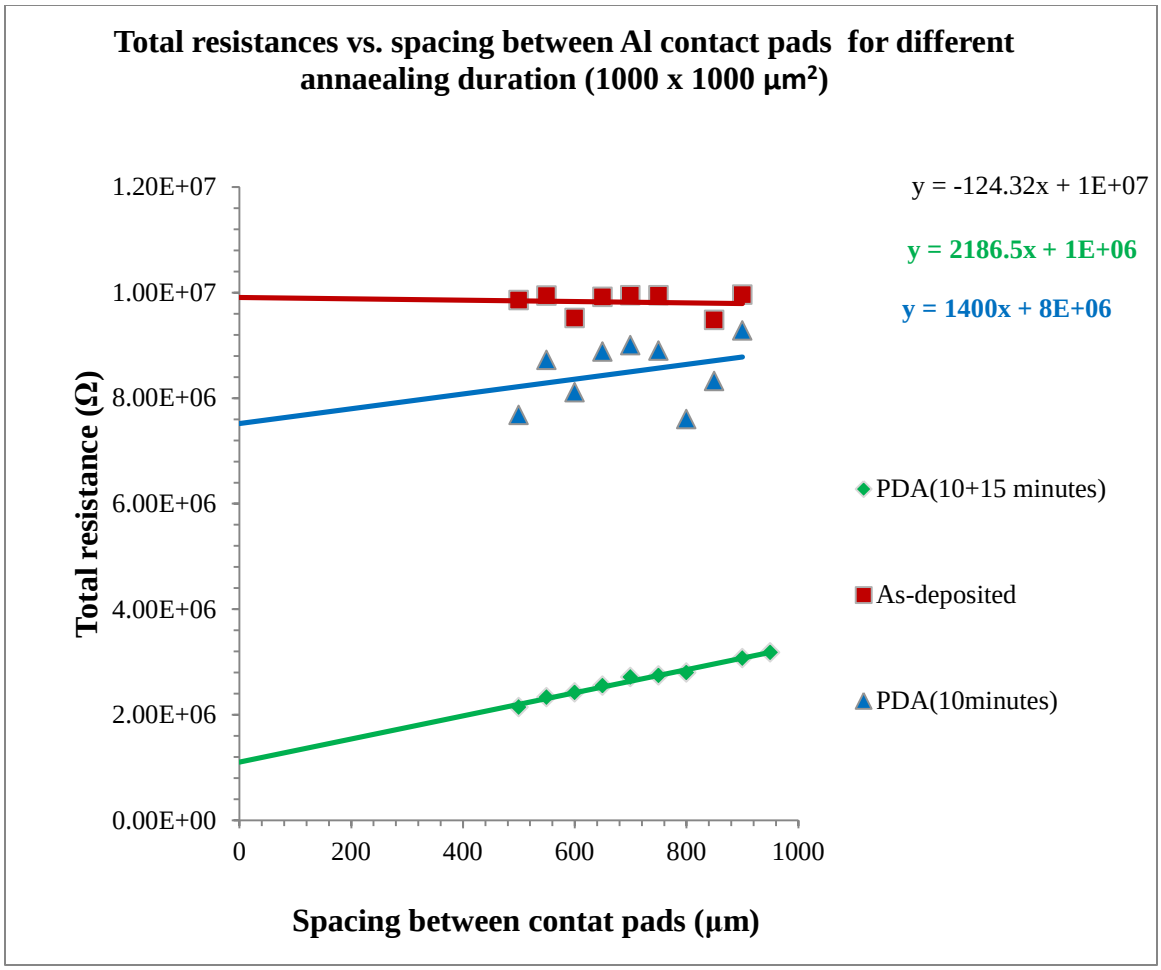

Figure 4.5 Total resistances vs. spacing between contact pads (1000 x 1000 µm^2) of Al contact scheme for different annealing duration

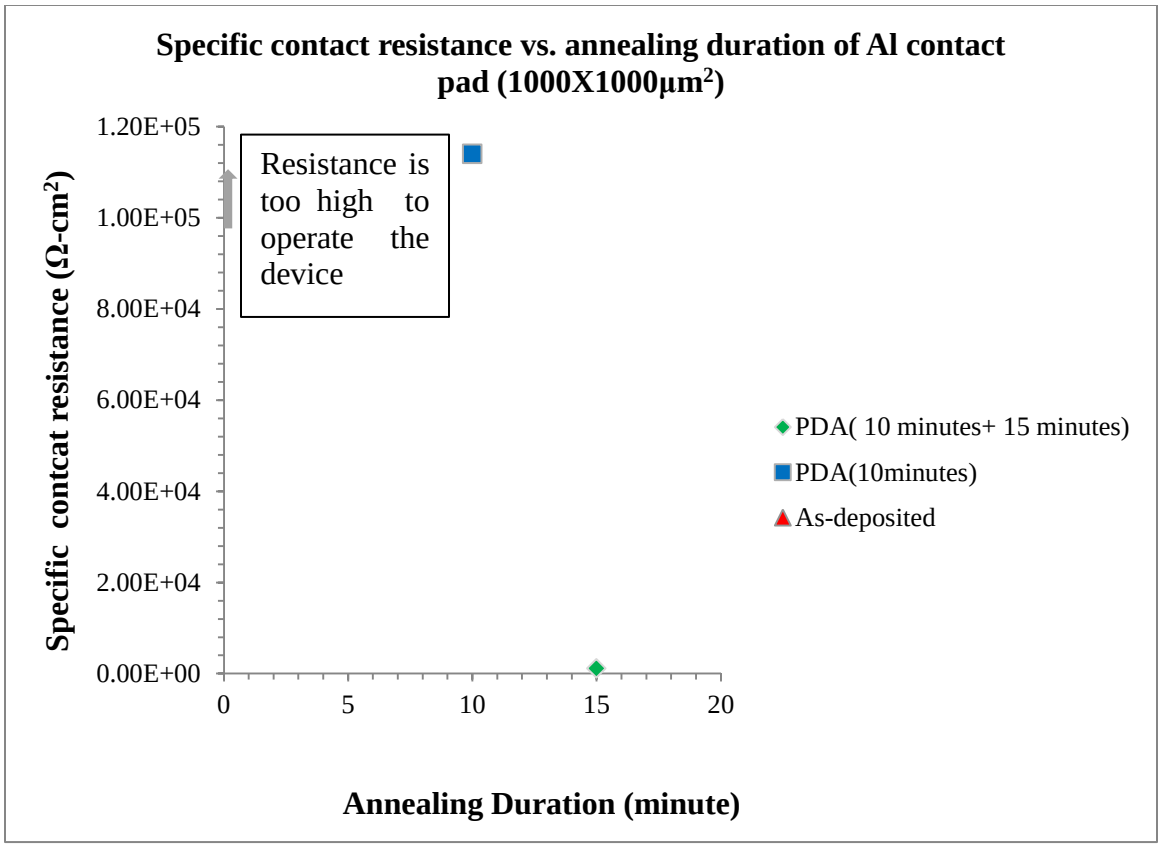

Figure 4.6. Specific contact resistance vs. annealing duration for Al contact (1000 x 1000µm^2) on GSZO film

Table 4.1. Transfer length measurements for Al contact on GSZO film

Contact Pad dimension	Annealing info	Transfer length (μm)	Contact resistance (R_c) (Ω)	Sheet resistance (R_s) (Ω/□)	Specific contact resistance (ρ_c) (Ωcm^2)
$300x300\mu m^2$	As-deposited	4.7×10^3	0.5×10^7	3.2×10^4	7×10^3
	PDA (10 minutes)	5.5×10^3	4.5×10^6	2.5×10^5	7×10^3
	PDA (10+ 15 minutes)	1.6×10^3	1.5×10^6	2.8×10^6	7.3×10^2
$500x500\mu m^2$	As-deposited	1.4×10^4	5×10^6	1.7×10^5	3.6×10^5
	PDA (10 minutes)	3.9×10^2	2.5×10^6	3.2×10^6	4.9×10^3
	PDA (10+15 minutes)	50	3.4×10^5	3.3×10^6	84
$1000x1000\mu m^2$	As-deposited	Not in the operable range			
	PDA (10 minutes)	2.9×10^3	4×10^6	1.4×10^6	1.1×10^6
	PDA (10+15 minutes)	2.3×10^2	5×10^5	2.2×10^6	1.1×10^3

4.1.2 Specific contact resistivity calculation of Ti (20 nm)/Al (30 nm)/Au (100 nm) contact on GSZO film

This section summarizes the resistance measurements results for contact pad size of 500 x 500 μm^2. The measurements have been done on as-deposited and post deposition annealed samples. Post deposition annealing has been performed for 7 minutes and then again for 15 minutes.

From figure 4.7, the transfer length is calculated as 1.6×10^3 μm .The values of contact resistance, sheet resistance and specific contact resistivity have also been calculated as 3.5×10^6 Ω, 1.08×10^6 Ω/□ and 2.8×10^4 Ω-cm^2.

Better contact resistance is obtained for the post deposition annealed contact than the as deposited one. The contact has been annealed for 7 minutes in nitrogen ambient. The value of contact resistance has reduced to 2 x 10^6 Ω. The slope of the trend line obtained from the plot (Figure 4.7) is 4 x 10^3 Ω/ μm .The slope is multiplied by the width of the contact pad that leads to the sheet resistance (2.05 x 10^6 Ω/□). The transfer length is calculated as 249 μm. The transfer length contributes to the calculation of specific contact resistance as actual contact area is determined by the transfer length. The sheet resistance is multiplied by the area of the effective contact region (L_T^2) to obtain the specific contact resistance. The specific contact resistivity (1.2 x 10^3 Ω-cm^2) is also decreased because of the reduction in transfer length as well as sheet resistance.

Another post deposition annealing of duration 15 minutes has been performed on the same contact to achieve a more conducting one. The contact resistance has been calculated from the intersecting point of y-axis in the plot (Figure 4.7) which is 1X10^6 Ω. The transfer length calculated from the intersecting point of the x-axis is 50.7 μm. The sheet resistance for this added annealing duration is 4.9 x 10^6 Ω/□. The value of specific contact resistivity is 126.8 which is less than the outcomes of previous annealing durations (as deposited and 7 minutes).

A further post deposition annealing of 15 minutes in the same ambient results more degradation in the contact resistance value. The contact has a resistance value of 3.7 x 10^5 Ω that has been extracted from the total resistance vs. spacing plot shown in Figure 4.7. The transfer length is 36.7 μm. The sheet resistance and specific contact resistivity are also dropped to 5.1 x 10^5Ω/□ and 68.6 Ω-cm^2, respectively.

The graphical comparison of specific contact resistivity against various annealing durations has been shown in Figure 4.8. The specific contact resistivity values have decreased with added post deposition annealing duration.

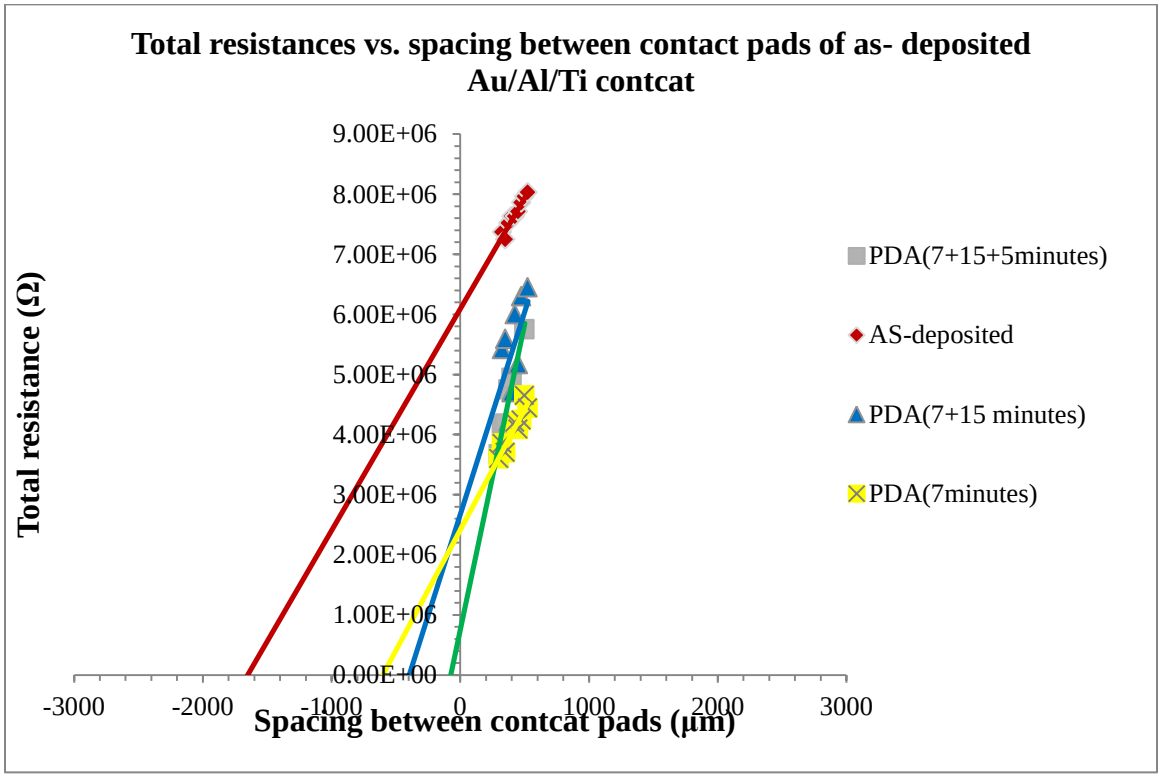

Figure 4.7 Total resistances vs. spacing between contact pads (500 x 500 µm^2) of Au/Al/Ti contact scheme for different annealing duration

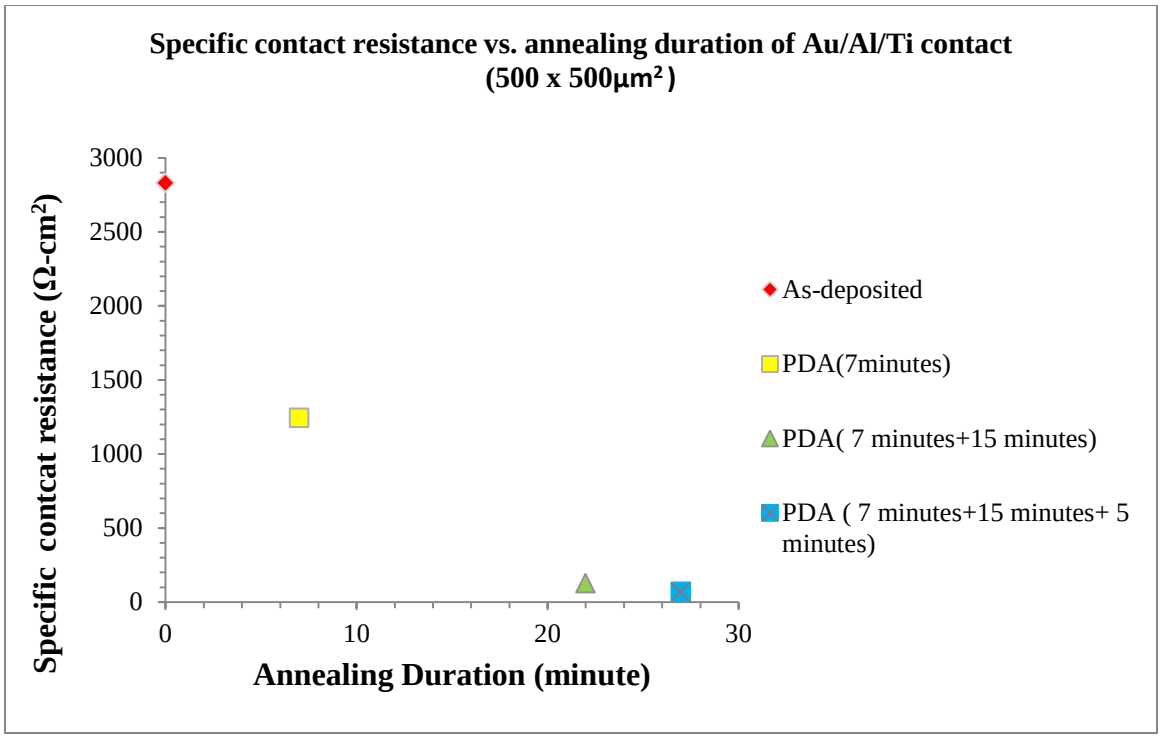

Figure 4.8. Specific contact resistance vs. annealing duration for Au/Al/Ti contact (500 x 500µm^2) on GSZO film

Table 4.2. Transfer length measurements for Au/Ti/Al contact on GSZO film

Contact Pad dimension	Annealing info	Transfer length (µm)	Contact resistance (R_c) (Ω)	Sheet resistance (R_s) (Ω/□)	Specific contact resistance (ρ_c) (Ωcm^2)
500X500µm^2	As-deposited	1.6 X 10^3	3.5 X 10^6	1 X 10^6	2.8 X 10^4
	PDA (7 minutes)	249	1 X 10^6	2 X 10^6	1.2 X 10^3
	PDA (7 +15 minutes)	50.7	1 X 10^6	4.9 X 10^6	126.8
	PDA (7+15+5 minutes)	36.7	3.7 X 10^5	5.1 X 10^5	68.6

4.1.3 Specific contact resistivity calculation of Al (30 nm)/Au (50 nm) contact on GSZO film

The dimensions of the Al/Au contact pad used for the measurements are 300 x 300 μm^2. The contact resistance and transfer length values calculated from Figure 4.9 are 0.5 x 10^7 Ω and 1.5 x 10^5 μm, respectively. The sheet resistance value extracted from the slope and the width of the trend line is 1 x 10^5Ω/□. The specific contact resistivity thus calculated as 2.2 x 10^5Ω-cm^2.

A post deposition annealing of duration 10 minutes has been done on the as-deposited sample. The contact resistance value (4.6 x 10^3 Ω) is less than the as- deposited contact. The transfer length is also decremented to 1.8 x 10^3 μm (Figure 4.9). The sheet resistance and specific contact resistance are computed as 7.6 x 10^5 Ω/□ and 2 x 10^4 Ω-cm^2.

Another subsequent post deposition annealing (15 minutes) has been executed on the same contact. The graph (Figure 4.9) shows a smaller transfer length (640 μm). The contact and sheet resistance are determined as 4 x 10^6 Ω and 1.9 x 10^6 Ω/□, respectively. The specific contact resistivity value is 7.7 x 10^3 Ω-cm^2. A declination has been observed in the specific contact resistivity value from the values of other annealing duration.

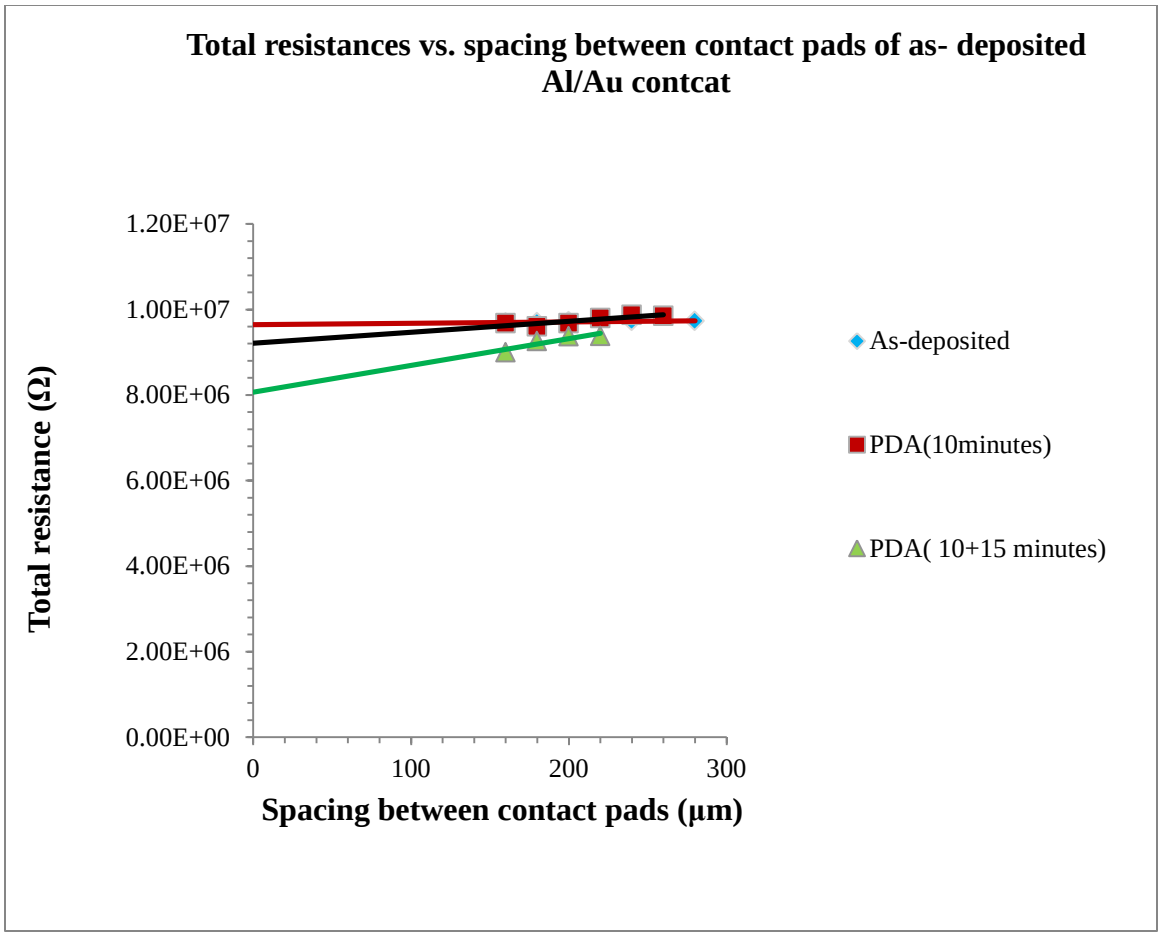

Figure 4.9. Total resistances vs. spacing between contact pads (300 X 300 µm^2) of Al/Au contact scheme for different annealing duration

The specific contact resistivity value is reduced with the incremental post deposition annealing duration shown in Figure 4.10. The behavioral trend of the Al/Au contact with respect to the increased post deposition annealing duration is similar to the other contacts shown in the previous sections. Post deposition annealing improves the contact quality and hence increases the current thorough the contacts. Another contact Al/Pt is also investigated to show the impact of the post deposition annealing.

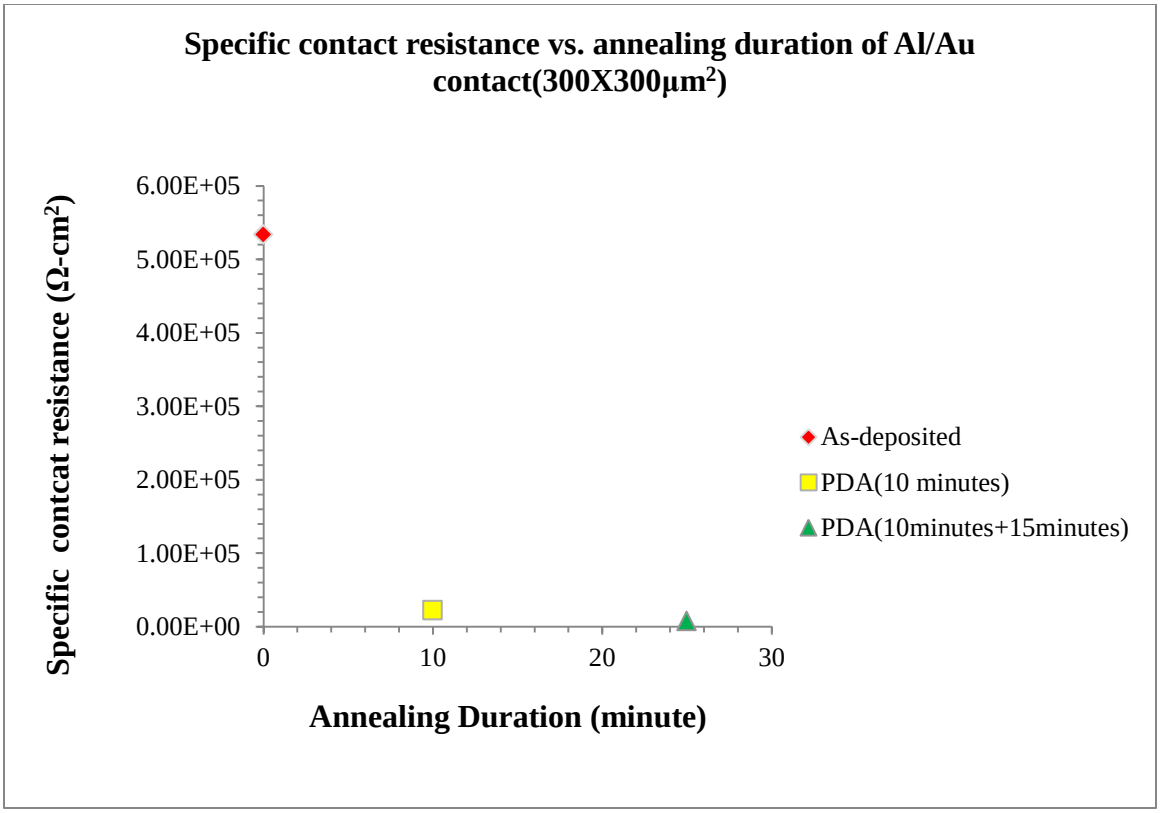

Figure 4.10. Specific contact resistance vs. annealing duration for Al/Au contact (300 x 300µm^2) on GSZO film

Table 4.3. Transfer length measurements for Al/Au contact on GSZO film

Contact Pad dimension	Annealing info	Transfer length (µm)	Contact resistance(R_c) (Ω)	Sheet resistance (R_s) (Ω/□)	Specific contact resistance (ρ_c) (Ωcm^2)
300X300µm^2	As-deposited	1.5 X 10^5	0.5 X 10^7	1 X 10^5	2.2 X 10^5
	PDA (10 minutes)	1.8 X 10^3	3 X 10^6	7.6 X 10^5	2 X 10^4
	PDA (10+ 15 minutes)	640	4 X 10^6	1.9 X 10^6	7.7 X 10^3

4.1.4 Specific contact resistivity calculation of Al(30 nm)/Pt (50 nm) contact on GSZO film

The dimension of the contact pad used for the measurements is 1000 x 1000μm^2. The contact resistance computed for the as-deposited contact is 3.5 x 10^6 Ω. The transfer length is found as 1 x 10^3 μm. The slope of the trend line (Figure 4.11) is 3.4 x 10^3 μm. The sheet resistance extracted from the slope and width of the contact pad is 3.4 x 10^5 Ω/□. The value of the specific contact resistance is 3.6 x 10^4 Ω-cm^2.

The measurements done on the post deposition annealed (15 minutes) sample reveal the contact, sheet and specific contact resistances as 2 x 10^6 Ω (Figure 4.11), 6.1 x 10^6 Ω/□ 6.5 x 10^3 Ω-cm^2, respectively The specific contact resistivity value is decreased compared to the as- deposited sample.

The specific contact resistivity has been calculated for subsequent post deposition annealing of 15 minutes. The contact resistance (2.5 x 10^6 Ω), sheet resistance (3.8 x 10^5 Ω/□and specific contact resistivity (1.6 x 10^3 Ω-cm^2) values are decremented from the as as-deposited and post deposition annealed (only 10 minutes) contact. The behavior of the contact for different annealing duration is shown in (Figure 4.12). The specific contact resistivity values are declining with the added post deposition annealing durations.

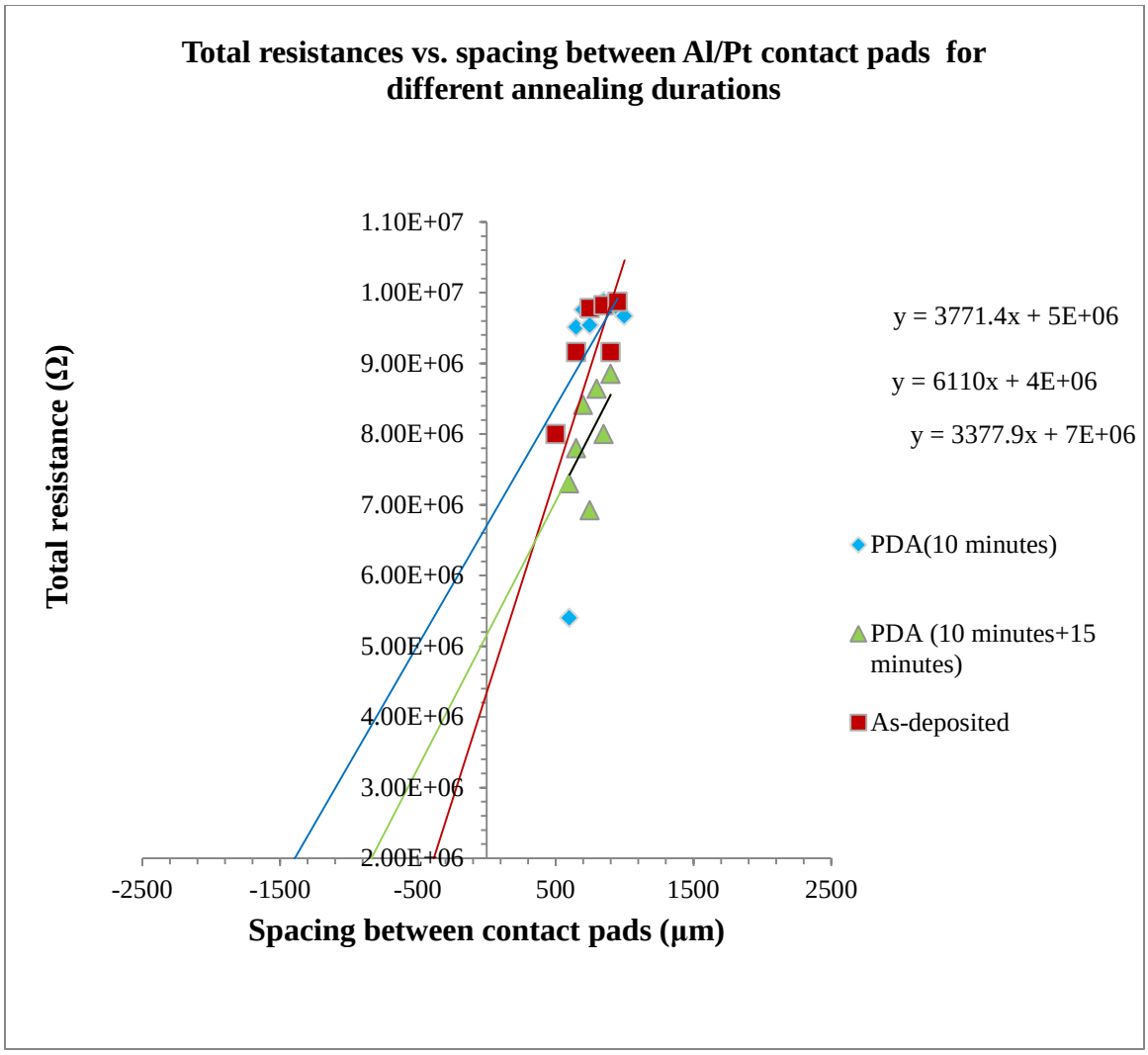

Figure 4.11. Total resistances vs. spacing between contact pads (1000 x 1000 µm^2) of Al/Pt contact scheme for different annealing duration

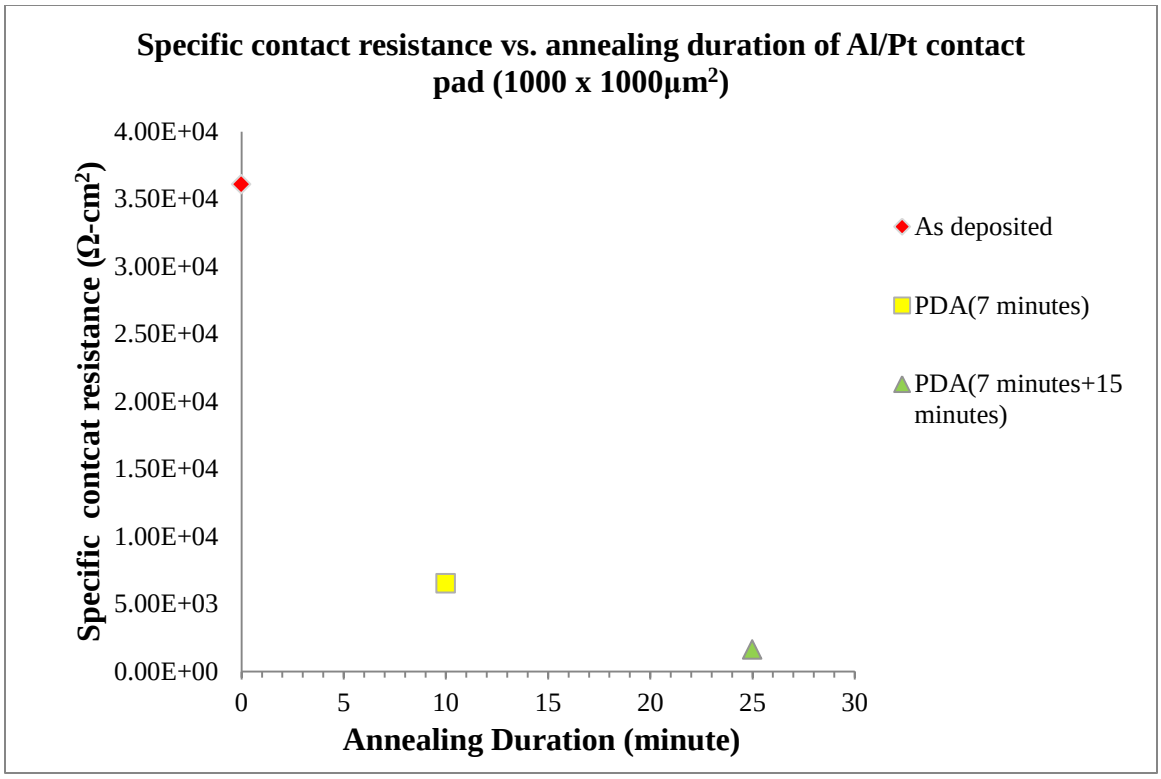

Figure 4.12. Specific contact resistance vs. annealing duration for Al/Pt contact (1000 x 1000 µm^2) on GSZO film

Table 4.4 Transfer length measurements for Al/Pt contacts on GSZO film

Contact Pad dimension	Annealing info	Transfer length (µm)	Contact resistance(R_c) (Ω)	Sheet resistance (R_s) (Ω/□)	Specific contact resistance (ρ_c) (Ωcm^2)
1000 x 1000µm^2	As-deposited	1.x 10^3	3.5 X 10^6	3.4 X 10^5	3.6 X 10^4
	PDA (10 minutes)	327	2 X 10^6	6.1 X 10^6	6.5 X 10^3
	PDA (10+ 15 minutes)	6.7 x 10^3	2.5 X 10^6	3.8 X 10^5	1.6 X 10^3

4.1.5 Current-voltage (I-V) characteristics of Al (100 nm) contact on GSZO film

The current-voltage characteristics of Al contact is shown in Figure 4.13. As-deposited contact reveal linear I-V behavior with specific contact of 7 x $10^3\Omega$-cm^2. Both post deposition annealed contacts of different duration show linear behavior with specific contact resistivities of around 7 x $10^3\Omega$-cm^2 and 726.9Ω-cm^2, respectively. The I-V characteristics are improved with increased post deposition annealing time.

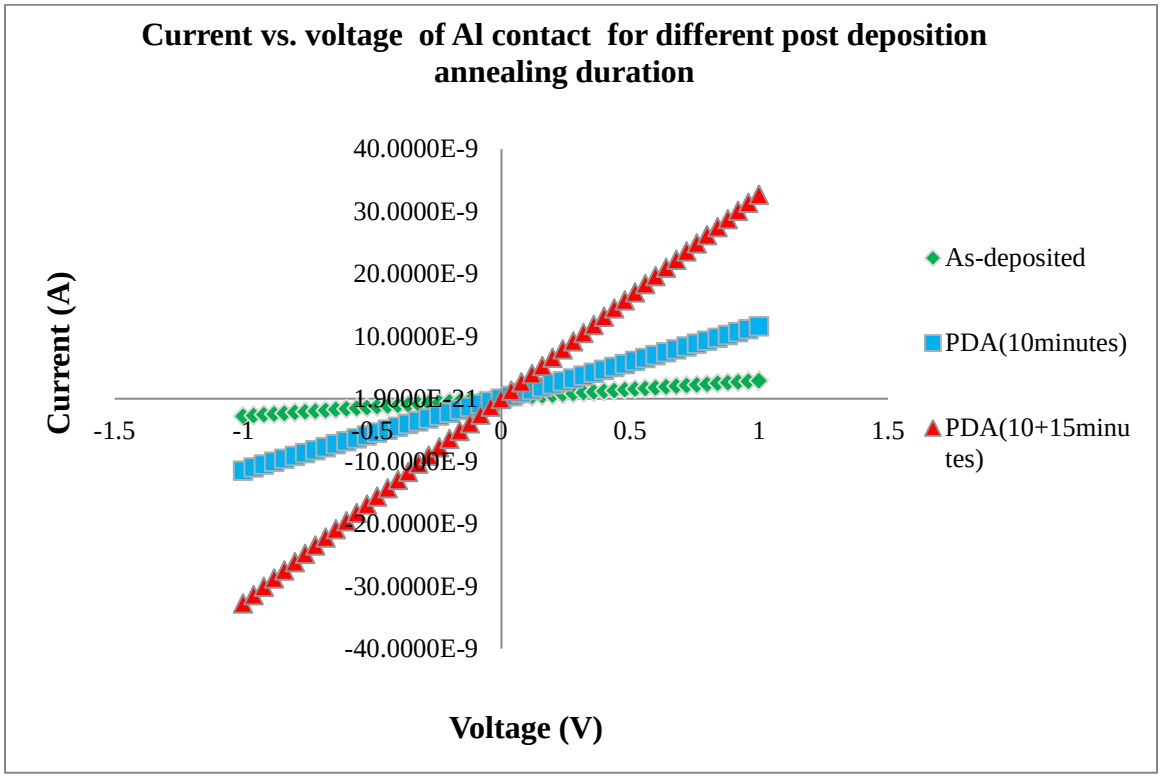

Figure 4.13. I-V characteristics of Al (300 x 300µm^2) contact on GSZO film

4.2 Thin Film Transistor Processing

The desired TFT layout can be achieved by controlling the parameters appropriately at different stages of processing. The proper fabrication of the TFT is the key component to get the intended characteristics. A small change in the fabrication process makes a large difference to the performance of the TFTs.

The photolithography process is very important as the basic patterns of the TFTs are formed after the lithography process. The spinning speed for the photoresist application affects the performance of the fabrication because the resist layer thickness can be controlled by spinning speed and time. The spinning speed was set initially 5000 rotation per minute for a duration of 30 seconds for HDMS and positive photo-resist as well as negative photo-resist coatings. This speed negatively affected the TFT characteristics because the positive photo-resist layer was not thick enough to protect the underlying layers from the subsequent steps. When the etching process was performed, some portion of the active layer (GSZO) was etched off that led the device to an inoperable state. As a result the spinning speed was decreased to 3000 rotation per minute to increase the photo-resist thickness.

The film developing times in the photolithography part have been tried are 1 minute, 2 minutes, 30 seconds and 45 seconds as shown in Figure 4.14. For, 30 seconds, 45 seconds and 1 minute development durations, the latent image is converted to the final image properly. When samples are developed for 2 minutes, the pattern dimensions are deteriorated.

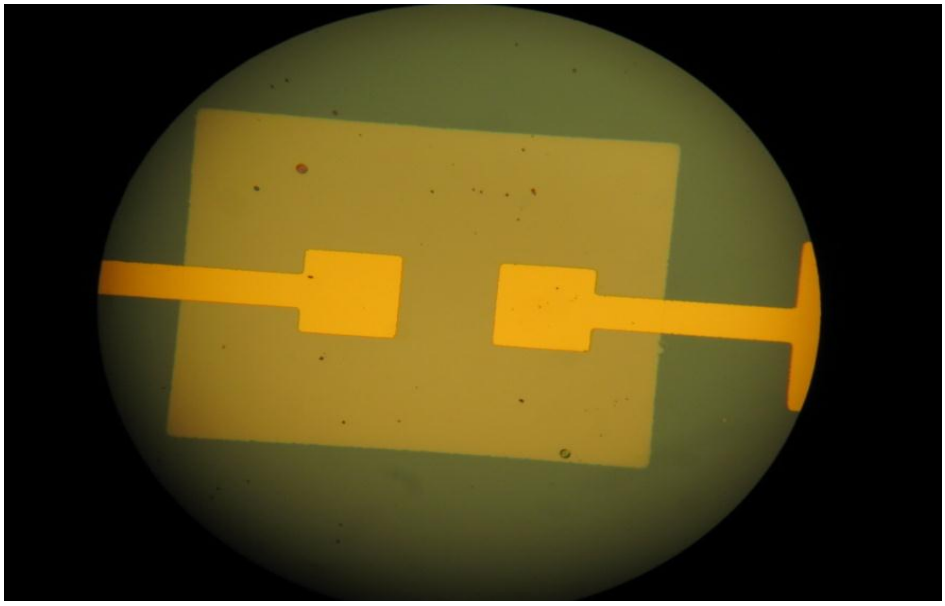

(a)

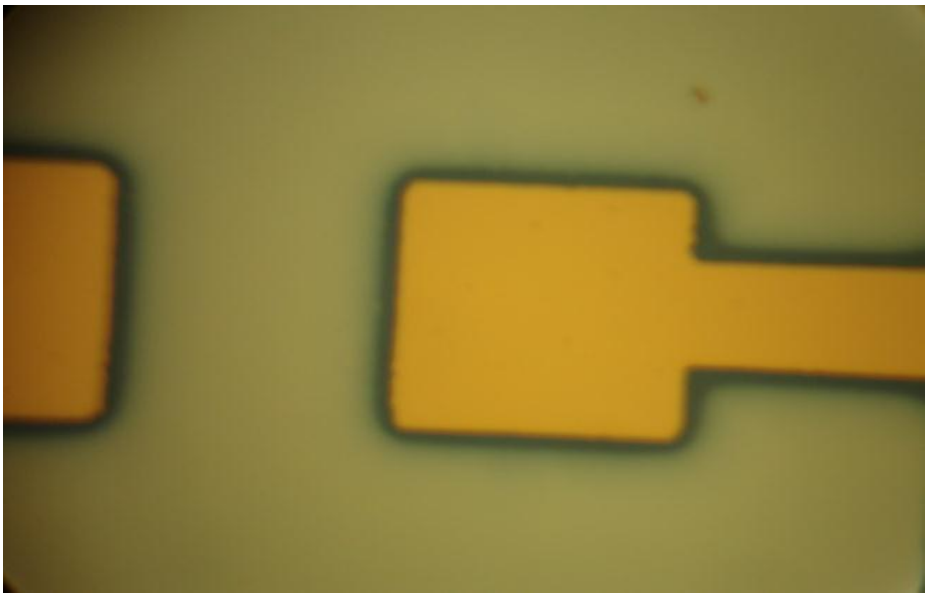

(b)

Figure 4.14. Views of TFTs differentiated by developing time: (a) pattern for 30 seconds developing time and (b) pattern for 2 minutes

In the etching process, proper determination of chemical amount and etching time are very important in the production of TFTs. The etching was done for 2 minutes by a mixture of 0.2 mL of HCl acid diluted with 100 mL of water .The performances of the TFTs etched for 30 seconds by a mixture 0.1 mL of HCl acid and 100 mL of DI water were unsatisfactory. If the resist coating is not thick enough, the subsequent layers get attacked by the acid. Some portion of the GSZO film underneath the resist coating is thus also etched off . As a result, the metal will be in contact with the oxide layer to some extent and contact quality between the metal and the film becomes poor. Hence, the etching time is reduced to 15 seconds. Figure 4.15 shows the complete removal of the resist layer because of the performance of the etching process for excessive period of time. But the photoresist should stay on the pattern and protect the underlying GSZO layer from the etching process.

Figure 4.15. Effect of excessive etching on the fabrication of TFTs

Plasma cleaning is done before the metal deposition to remove the water contaminant raised from the photolithography process. Plasma cleaning was not performed for the first few TFTs. As the coated sample is cleaned with water after development, the water particles are left over the samples. The contact after metal deposition becomes poor because of this water particle. The moderate time for plasma cleaning is set for 5 minutes. Plasma cleaning has removed the water particle by reducing the surface energy of the water particle to the surface. The contact angle measured before the plasma cleaning is close to 26^{o}. The water particles spread out on the surface which is shown in Figure 4.16 (a). The contact angle has been improved which approximately 70^{o} after plasma is cleaning. The water droplet is not now totally spread over the surface as before.

(a)

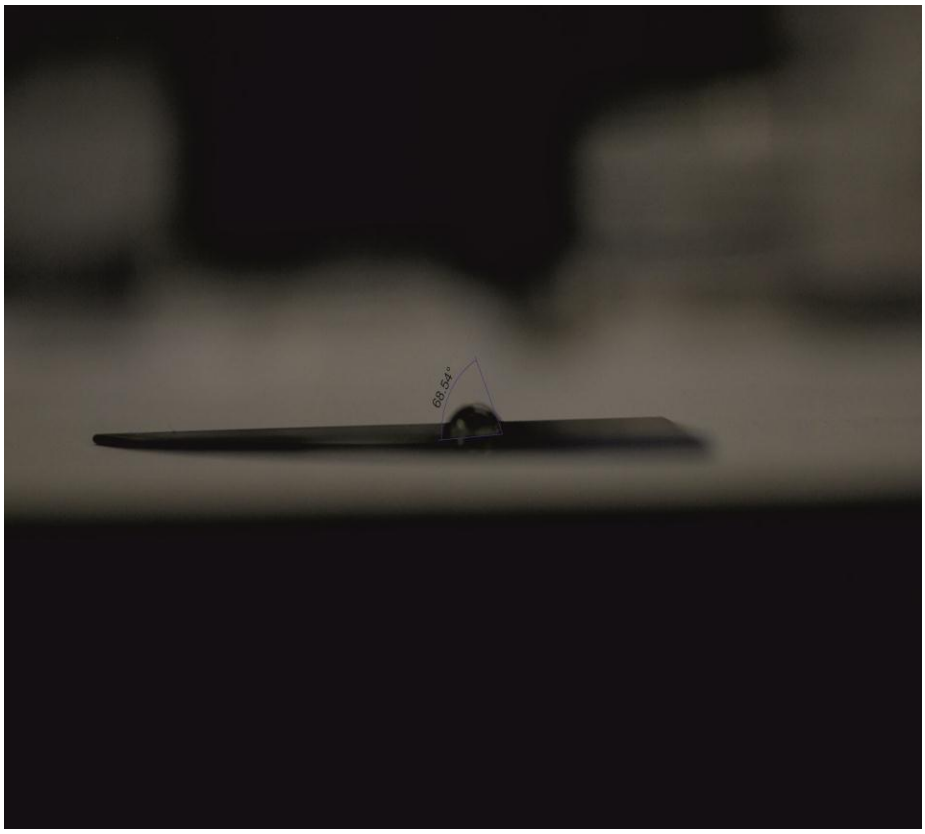

(b)

Figure 4.16. Change in the contact angle of the water droplet by plasma cleaning: (a) small contact angle before cleaning and (b) improved contact angle after cleaning

As the plasma cleaning is carried out in oxygen ambient, the sample color also changes. The changes in the sample color are shown in Figure 4.17. In the plasma cleaning method, oxygen gas enters into the chamber and from oxygen plasma. The plasma undergoes in reaction with the water particles on the surface and removes OH groups. As the chemical reaction happens between the plasma and the water particle, the color of the surface gets changed.

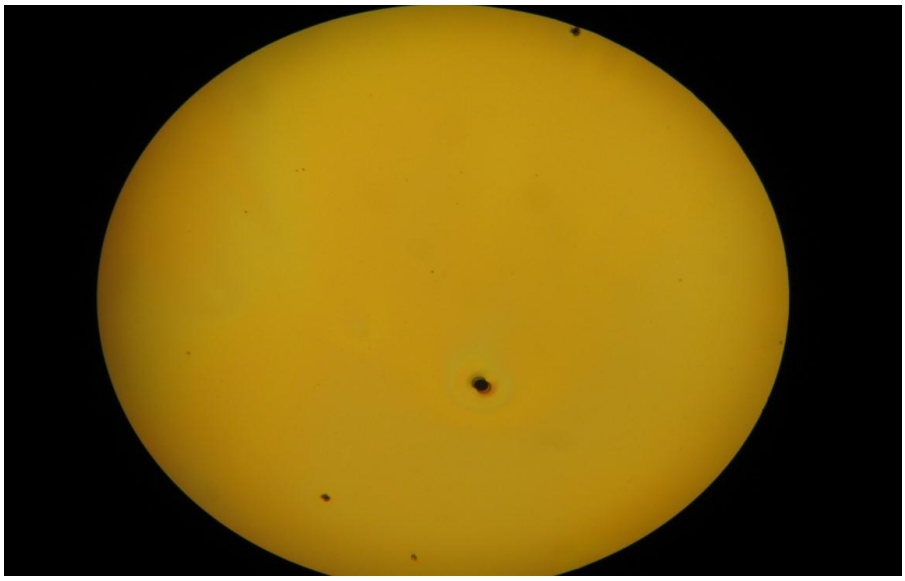

(a)

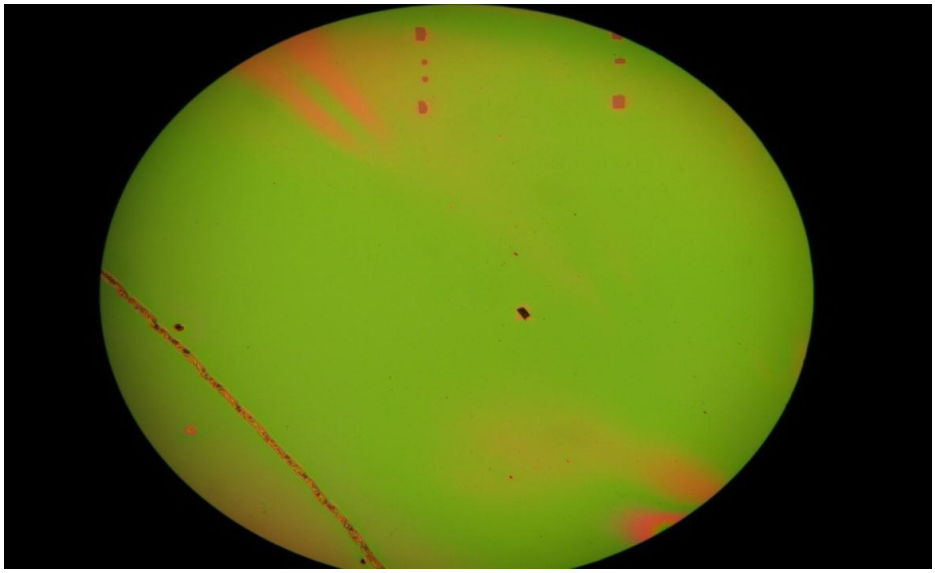

(b)

Figure 4.17. Plasma cleaning done on Si wafer: (a) before plasma cleaning and (b) change in color after plasma cleaning

The metal deposition has been started with very high deposition rate like 40 Å/ second or 35 Å/second. The problem with such a fast deposition rate is the metal does not get attached firmly with the surface. The metal gets flaked off when the probe is set on the metal for characterization. As a result, the deposition rates are reduced to 5 Å/second and 1 Å/second for Ti and Au , respectively.

To lift off the metal, only acetone and propanol were used at the beginning, The acetone and propane did not work initially because the metal in the crucible of electron beam evaporation system was oxidized due to the metal being inside the system for a long period of time shown in Figure 4.18 (a). After loading the fresh metal, acetone and propanol could remove the metal properly. But the metal particle still remained on the samples even after rinsing with water. This problem was solved by using the chemical n-methyl-2-pyrrolidone (NMP). NMP cleans metal dots completely on the surface of the sample presented in Figure 4.18 (b).

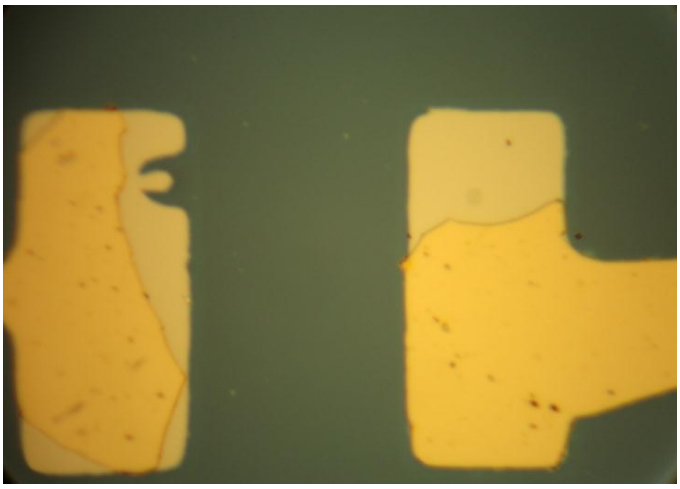

(a)

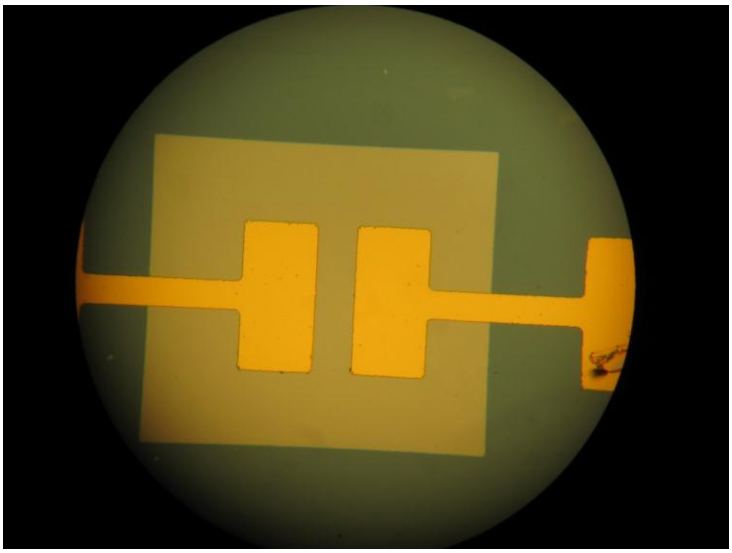

(b)

Figure 4.18. Difference between unsuccessful successful lift-off processes: (a) unsuccessful removal of metal and (b) proper removal of metal from the intended areas of the pattern and wafer

4.3 Discussion

The post deposition annealing duration dependence of specific contact resistivity for various metallization patterns are demonstrated in this work. Among all the contacts examined, Al (100 nm) produces the best results in the shortest period of annealing time. The linear I-V characteristics indicates an ohmic contact with specific contact resistivity of 84 Ω-cm^2 for the post deposition annealing duration of 10 minutes followed by another 15 minutes annealing. The resistivity is lowered from the as-deposited contact (3.6 x 10^5 Ω-cm^2) after post deposition annealing as the interfacial reactions [2] gets accelerated by this process. The reactions lead to the out diffusion of oxygen from the GSZO films to the Al layer. Hence Al_2O_3 [2] is formed easily as the formation enthalpy is very less for Al_2O_3 (ΔH_{Al2O3}= -1676 KJ/mole [1]. This out diffusion process of oxygen yields to the oxygen vacancy as well as an addition to the carrier concentration in the GSZO active

layer [2]. An in diffusion of Al to the active layer may happen that will also increase the carrier concentration. The electrical property is thus improved by the optimal exhibition of post deposition annealing.

Ti (20 nm)/Al (30 nm)/Au (100 nm) contact also possess lower contact resistivity than the Al (30nm)/Au(50nm) and Al(30nm)/Pt(50nm) contacts. This contact has the specific contact resistivity of 68.6 Ω-cm^2 after three subsequent post depositions annealing of duration 7, 15 and 5 minutes. TiO and TiO_2 compounds are formed by the oxygen out diffusion [38] in the interfacial reactions. The oxygen vacancy is thus created and the carriers as well as the resistivity are improved. The oxygen may diffuse to the Al through the Ti layer. The oxygen vacancy created in the GSZO thus should be less compared to the Al (100nm) as Ti oxides have smaller enthalpy [TiO (ΔH_{TiO}= -944 KJ/mole) and TiO_2 (ΔH_{TiO2}= -519 KJ/mole)] compared to the Al_2O_3. Therefore, the Ti/Al/Au attains approximately similar resistivity for higher duration (27 minutes) of post deposition annealing.

The Al(30 nm)/ Au(50nm) and Al (30nm)/Pt(50nm) provide specific contact resistivity of 7.7 x 10^3 Ω-cm^2 and 1.6 x 10^3 Ω-cm^2 , respectively and exhibit poor electrical property in comparison to the contacts analyzed above..

According to the literature review, the specific contact resistivity of Al/Pt and Al/Au contact should perform better than Al as well Ti/Al/Au contact. But our result shows Al as the best performing contact. This we attribute to the e non removal of contaminants in the different steps of photolithography. Oxygen plasma cleaning was applied in case of Al and Ti/Al/Au contacts, before metal deposition to remove the water particle. But the

metal was deposited directly after development for other two contacts (Al/Pt and Al/Au) as the plasma cleaning system developed some serious problems. The results demonstrate the necessity of application of plasma cleaning before metal deposition to ensure good contact quality.

Cleanliness in very important for successful fabrication of TFTs. Even though the wafers are cleaned ultrasonically with trichloroethylene, acetone and propanol, the water particles are still problems that degrade the contact quality and hinder the device improved performance. The spinning speed and time for resist coating are 3000 r.p.m and 30 seconds to maintain the proper thickness of the wafer. The soft baking time and temperature are 1 minute and 90^{o}C, respectively. The wafers are exposed to ultraviolet ray typically for 30 seconds to get the latent image and developed for 30 seconds to convert the latent image to the real one. It is to be noted that higher development time of 1 minute was also satisfactory, though the standard time period of 15 seconds for etching showed better results compared to the other attempted intervals. Plasma cleaning is performed for 5 minutes to remove the water particle and to make the surface smooth for metal deposition. The metals were deposited by electron beam evaporation for better uniformity as well as it allows sequential depositions of the metals.

CHAPTER 5

CONCLUSION AND FUTURE WORK

5.1 Conclusion

Among all metallization design investigated, Al (100 nm) provides the best resistivity in the shortest annealing period. Results show that Al has contact resistivity of 84 Ω-cm^2 for contact pad size of 500 x 500 μm^2 for consecutive post deposition annealing of 10 minutes and 15 minutes. A decreasing trend in the contact resistivity is observed with increased post deposition annealing temperature. The same tendency is followed in the specific contact resistivity behavior for other pad sized of 300 x 300 μm^2 and 1000 x 1000 μm^2. Although Ti/Al/Au contact also establishes improved specific contact resistivity of 68.6Ω-cm^2 and resistivity is reduced with added post deposition annealing temperature, the trend is not consistent for other contact pad sizes (300 x 300 μm^2 and 1000 x 1000 μm^2). The Al (30 nm)/ Au(50nm) and Al (30nm)/Pt(50nm) contacts show very poor conductivity with high specific contact resistivity of 7.7 x 10^3 Ω-cm^2 and 1.6 x 10^3 Ω-cm^2 respectively. Thus Al appears to be the best contact for GSZO from the above studies not only from the electrical properties but also from simplicity as only a single element is involved for the contact.

The parameters of different processing steps are determined after various experimental trials and maintained the same throughout the fabrication method. The device performances can still be improved The device performances can still be improved

if carried out in a clean room better than class 10,000 environment, that has been done for this work and the use of better cleaning procedures for the wafers.

5.2 Future Work

It was found the plasma cleaning is important prior to metal deposition for a better electrical contact, couple of metal schemes where plasma cleaning was not performed needs to be repeated. Other additional steps such as a short duration dehydration baking to be carried out at 150^{o} C for 1 minute [42] before priming with HDMS is also expected to remove the water particle from the surface and hence improve the adhesion. The negative photoresist developer used for the lithography process in an organic solvent based bis-arilaize. The samples studied in this thesis were cleaned after development only with water. Including an intermediate step of rinsing with another organic solvent such as n-butlyl acetate [42] as negative resist developer, being an organic solvent is also expected to improve the water removal from the surface. In this work only I-V characteristics have been carried out to verify the contact quality.. The Auger electron spectroscopy (AES) and x-ray photo electron spectroscopy of the interface would provide more insight into the physical mechanism responsible for the observed electrical behavior.

REFERENCES

1. Kim, H.-K. and J.-M. Lee, *Low resistance nonalloyed Al-based ohmic contacts on n-ZnO:Al.* Superlattices and Microstructures, 2007. **42**(Compendex): p. 255-258.

2. Kim, H.-K., et al., *Formation of low resistance nonalloyed Al/Pt ohmic contacts on n-type ZnO epitaxial layer.* Journal of Applied Physics, 2003. **94**(Compendex): p. 4225-4227.

3. Kim, H.-K., et al., *Low-resistance Ti/Au ohmic contacts to Al-doped ZnO layers.* Applied Physics Letters, 2000. **77**(Compendex): p. 1647-1649.

4. Kim, H.-K., et al., *Study of the Electrical and Structural Characteristics of Al/Pt Ohmic Contacts on n-Type ZnO Epitaxial Layer.* Journal of the Electrochemical Society, 2004. **151**(Compendex): p. G223-G226.

5. Nomura, K., et al., *Room-temperature fabrication of transparent flexible thin-film transistors using amorphous oxide semiconductors.* Nature, 2004. **432**(Compendex): p. 488-492.

6. Carey, P.G., et al. *Polysilicon TFT fabrication on plastic substrates*. in *Proceedings of the 1997 17th Annual International Display Research Conference, September 15, 1997 - September 19, 1997*. 1997. Toronto, Can: SID.

7. Nomura, K., et al., *Room-temperature fabrication of transparent flexible thin-film transistors using amorphous oxide semiconductors.* Nature, 2004. **432**(7016): p. 488-492.

8. Erskine, J.C. and A. Cserhati, *Cadmium selenide thin-film transistors.* 1978. **15**(Compendex): p. 1823-1835.

9. Hoffman, R.L., B.J. Norris, and J.F. Wager, *ZnO-based transparent thin-film transistors.* Applied Physics Letters, 2003. **82**(Compendex): p. 733-735.

10. M. K. Fung, et al. *Influence of the film thickness on the optical and electrical properties of ITO*. in *Mater. Res. Soc. Symp. Proc., vol. 1212*. 2010.

11. Fortunato, E., et al. *New amorphous oxide semiconductor for thin film transistors (TFTs)*. in *Advanced Materials Forum IV - Selected, peer reviewed papers from the 4th International Materials Symposium Materiais 2007 and 8th Encontro da Sociedade Portuguesa de Materiais - SPM, April 1, 2007 - April 4, 2007*. 2008. Porto, Portugal: Trans Tech Publications Ltd.

12. Fortunato, E.M.C., et al., *High mobility indium free amorphous oxide thin film transistors.* Applied Physics Letters, 2008. **92**(Compendex).

13. Braun, F., *On the Conduction Through Sulfurmetals (in German).* Annal. Phys. Chem, 1874. **153**: p. 556-563.

14. Oussalah, S., B. Djezzar, and R. Jerisian, *A comparative study of different contact resistance test structures dedicated to the power process technology.* Solid-State Electronics, 2005. **49**(10): p. 1617-1622.

15. Kamimura, K., et al., *Characterization of contact resistance of low-value resistor by Transmission Line Model (TLM) method.* Electronics and Communications in Japan, Part II: Electronics (English translation of Denshi Tsushin Gakkai Ronbunshi), 2002. **85**(Compendex): p. 16-22.

16. Mohney, S.E., et al., *Measuring the specific contact resistance of contacts to semiconductor nanowires.* Solid-State Electronics, 2005. **49**(Compendex): p. 227-232.

17. Chern, J.G.J. and W.G. Oldham, *Determining specific contact resistivity from contact end resistance measurements.* Electron device letters, 1984. **EDL-5**(Compendex): p. 178-180.

18. Berger, H.H., *Models for contacts to planar devices.* Solid-State Electronics, 1972. **15**(2): p. 145-158.

19. Xu, Y., et al., *Modified transmission-line method for contact resistance extraction in organic field-effect transistors.* Applied Physics Letters, 2010. **97**(Compendex).

20. Cox, R.H. and H. Strack, *Ohmic contacts for GaAs devices.* Solid-State Electronics, 1967. **10**(12): p. 1213-1214, IN7-IN8, 1215-1218.

21. Murrmann, H. and D. Widmann, *Current crowding on metal contacts to planar devices.* 1969(Compendex): p. 162-163.

22. Proctor, S.J., L.W. Linholm, and J.A. Mazer, *Direct measurements of interfacial contact resistance, end contact resistance, and interfacial contact layer uniformity.* IEEE Transactions on Electron Devices, 1983. **ED-30**(Compendex): p. 1535-1542.

23. Shih, K.K. and J.M. Blum, *Contact resistances of Au-Ge-Ni, Au-Zn and Al to III-V compounds.* Solid-State Electronics, 1972. **15**(Compendex): p. 1177-1180.

24. Schroder, D.K., *Semiconductor Material And Device Characterization* ,. 1990, 128-129 New York: Wiley Interscience.

25. chen, K.X., et al. *Four-point TLM measurement for specific contact resistance assessment*.

26. Sullivan, M.V. and J.H. Eigler, *Five Metal Hydrides as Alloying Agents on Silicon.* Journal of the Electrochemical Society, 1956. **103**(4): p. 218-220.

27. Hsu, S.T., *Noise in high-gain transistors and its application to the measurement of certain transistor parameters.* Electron Devices, IEEE Transactions on, 1971. **18**(7): p. 425-431.

28. Ting, C.-Y. and C.Y. Chen, *A study of the contacts of a diffused resistor.* Solid-State Electronics, 1971. **14**(6): p. 433-438.

29. Shepela, A., *Specific contact resistance of Pd2Si contacts on n- and p-Si.* Solid-State Electronics, 1973. **16**(Compendex): p. 477-481.

30. Schroder, D.K., *Semiconductor Material And Device characterization*. 1990, 110-114, New York: Wiley Interscience.

31. Kennedy, D.P. and P.C. Murley, *A two-Dimensional Mathematical Analysis of the Diffused Semiconductor Resistor.* IBM J. Res. Dev, May 1968. **12**: p. 242-250.

32. Neamen, D., *Semiconductor Physics And Devices*. 2011: McGraw-Hill Companies,Inc.

33. Murrmann, H. and D. Widmann, *Measurement of the Contact Resistance Between Metal and Diffused Layer in Si Plannar Devices (in German).* Solid-State Electronics, Dec.1969. **12**: p. 879-886.

34. Berger, H.H., *Contact Resistance and Contact Resistivity.* J. Electrochem. Soc., Feb.1972. **119**: p. 507-514.

35. Schuldt, S.B., *An Extra Derivation of Contact Resistance to Plannar Devices* Solid-State Electronics, May. 1978. **21**: p. 715-719.

36. Shockley, W., A. Goetzberger, and R.M. Scarlett, *Research and Investigation of Inverse Epitaxial UHF Power Transistors*. Sept.1964: Air Force Avionics Lab., Wright-Patterson Air Force Base, OH, .

37. Lin, G.-R. and S.C. Wang, *Comparison of high-resistivity ZnO films sputtered on different substrates.* Japanese Journal of Applied Physics, Part 2: Letters, 2002. **41**(Compendex): p. L398-L401.

38. Kim, H.-K., et al., *Electrical and Structural Properties of Ti/Au Ohmic Contacts to n-ZnO.* Journal of the Electrochemical Society, 2001. **148**(3): p. G114-G117.

39. Wager, J.F., D.A. Keszler, and R.E. Presley, *Transparent Electronics,* . 2008, New york: Springer.

40. Martins, R., et al., *Role of order and disorder on the electronic performances of oxide semiconductor thin film transistors.* Journal of Applied Physics, 2007. **101**(Compendex).

41. Yabuta, H., et al., *High-mobility thin-film transistor with amorphous InGaZnO4 channel fabricated by room temperature rf-magnetron sputtering.* Applied Physics Letters, 2006. **89**(Compendex).

42. *Silicon Processing*: ASTM International.

43. belkind, A. and S. Gershman *Plasma Cleaning of Surfaces*.

44. *Fabrication techniques*. Available from: http://www.ece.utep.edu/research/cdte/Fabrication/index.htm.